Golgb1 regulates protein glycosylation and is crucial for mammalian palate development

Yu Lan[1,2] *, Nian Zhang[2], Han Liu[2], Jingyue Xu[2], Rulang Jiang[1,2]

[1] Division of Plastic Surgery, Cincinnati Children's Hospital Medical Center, Cincinnati, OH 45229, USA

[2] Division of Developmental Biology, Cincinnati Children's Hospital Medical Center, Cincinnati, OH 45229, USA

*Author for correspondence: Yu Lan, Ph.D.
Division of Plastic Surgery
Cincinnati Children's Hospital Medical Center
Cincinnati, OH 45229
USA
Telephone: (513) 803-7842
E-mail: Yu.Lan @cchmc.org

Keywords: cleft palate, craniofacial, CRISPR, ENU, glycosylation, genome editing, Golgi, mutation

Summary Statement

Through phenotype-driven genetic screening in mice, combined with whole exome sequencing for mutation discovery and CRISPR/Cas9-mediated genome editing for validation of causality, we have identified the vesicle tethering protein Golgb1 as a key regulator of protein glycosylation critical for mammalian palatogenesis.

Abstract

Cleft palate is a common major birth defect for which currently known causes account for less than 30% of pathology in humans. In this study, we carried out mutagenesis screening in mice to identify new regulators of palatogenesis. Through genetic linkage mapping and whole exome sequencing, we identified a loss-of-function mutation in the *Golgb1* gene that co-segregated with cleft palate in a new mutant mouse line. *Golgb1* encodes a ubiquitously expressed large coiled-coil protein, known as giantin, that is localized at the Golgi membrane. Using CRISPR/Cas9-mediated genome editing, we generated and analyzed developmental defects in mice carrying additional *Golgb1* loss-of-function mutations, which validated a critical requirement for Golgb1 in palate development. Through maxillary explant culture assays, we demonstrate that the *Golgb1* mutant embryos have intrinsic defects in palatal shelf elevation. Just prior to the developmental stage of palatal shelf elevation in the wildtype littermates, *Golgb1* mutant embryos exhibit increased cell density, reduced hyaluronan accumulation, and impaired protein glycosylation in the palatal mesenchyme. Together, these results demonstrate that, although it is a ubiquitously expressed Golgi-associated protein, Golgb1 has specific functions in protein glycosylation and tissue morphogenesis.

Introduction

In mammals, palatal shelves arise from the oral side of the maxillary prominences during embryogenesis and initially grow downward, flanking the developing tongue (Bush and Jiang, 2012; Lan et al., 2015). At a specific developmental stage, the palatal shelves re-orient to the horizontal position above the tongue, grow toward the midline and subsequently fuse with each other to form the roof of the oral cavity. Concurrent to palate development, the surrounding craniofacial structures undergo significant growth and morphogenesis. Cleft palate could result from intrinsic defects in palatal shelf growth, elevation, or fusion, or from failure of the palatal shelves contacting each other at the right developmental stage due to malformation of surrounding structures (Bush and Jiang, 2012; Gritli-Linde, 2007; Hilliard et al., 2005; Lan et al., 2015). Although extensive gene knockout studies in mice in the last 25 years have shown that all major signaling pathways, including Bmp, Fgf, Notch, Shh, Tgfβ, and Wnt pathways, play critical roles in palate development, mutations in known palate development regulators have been found in less than 30% of cleft palate patients (Bush and Jiang, 2012; Gritli-Linde, 2007; Hilliard et al., 2005; Lan et al., 2015; Moore and Persaud, 1998). Many more genes with critical roles in palate development remain to be discovered.

The Golgi is an intracellular organelle composed of a series of flattened membrane structures and functions as a carbohydrate synthesis and glycosylation factory at the crossroads of the secretory pathway (Mellman and Warren, 2000). Almost all signaling molecules and extracellular matrix (ECM) components are processed through the Golgi prior to arriving at the cell surface (Mellman and Warren, 2000; Zhong, 2011). In addition to containing a large number of enzymes that are responsible for catalyzing protein and lipid modifications, the Golgi houses many proteins that are involved in packaging, tethering, and transporting secretory vesicles (Linstedt and Hauri, 1993; Munro, 2011; Puthenveedu and Linstedt, 2001; Short et al., 2005; Zhong, 2011). Dozens of human developmental disorders and diseases have been associated with mutations in Golgi-associated proteins (Freeze and Ng, 2011; Smits et al., 2010). Remarkably, several mutations in genes encoding vesicle transport proteins cause craniofacial and skeletal disorders with distinct phenotypes (Follit et al., 2008; Freeze and Ng, 2011; Kim et al., 2012; Smits et al., 2010), which underscore the importance of understanding Golgi-mediated cell biological processes in the context of development (Freeze and Ng, 2011; Kim et al., 2012; Smits et al., 2010).

Golgb1, also known as giantin, is a Golgi-associated large transmembrane protein (Linstedt and Hauri, 1993). Golgb1 has been found to interact with the transcytosis associated protein p115, a cytosolic protein encoded by the *Uso1* gene involved in tethering ER-derived vesicles to the Golgi in mammalian cells as well as in yeast (Cao et al., 1998; Koreishi et al., 2013; Puthenveedu and Linstedt, 2001). Mouse embryos deficient in p115 exhibit early embryonic lethality and Golgi fragmentation in trophoblast cells (Kim et al., 2012). Although no *Golgb1* mutant mice have been reported, Katayama *et al.* recently identified a 10-bp insertion in exon-13 of the *Golgb1* gene in rats carrying a spontaneous *osteochondrodysplasia* (*ocd*) mutation (Katayama et al., 2011). The *ocd* homozygous mutant rats exhibit disproportionate dwarfism, systematic edema, cleft palate, and neonatal lethality (Katayama et al., 2011), but whether these developmental defects are caused by loss of Golgb1 function has not been validated and the cellular functions of Golgb1 *in vivo* remain to be characterized. In this study, we identify a splice donor site mutation in the *Golgb1* gene that completely co-segregates with a cleft palate phenotype in a new chemically induced mutant mouse line. We validate that loss of *Golgb1* function causes cleft palate in mice through generation and analysis of mice carrying additional *Golgb1* loss-of-function alleles by using CRISPR/Cas9-mediated genome editing. Furthermore, we demonstrate that Golgb1 plays a crucial role in protein glycosylation in the developing palatal mesenchyme cells. Our results provide novel insights into Golgi biology and the molecular and cellular mechanisms of palate development.

Results

Identification of an ENU-induced cleft palate mutation

We performed an N-ethyl-N-nitrosourea (ENU) mutagenesis screen in mice to identify new genes critical for mammalian organogenesis. Using a three-generation screening strategy designed to recover autosomal recessive mutations (Supplementary Fig. 1A), we screened E16.5-E18.5 embryos for structural defects in 12 G1 families. The *ENU1483* line produced embryos with cleft palate at high frequency (Supplementary Fig. 1B). SNP linkage analysis mapped the causal mutation to proximal Chromosome 16, in between 29 Mb to 50 Mb (Supplementary Table 1). Loss-of-function mutations in two genes, *Gsk3b* and *Dlg1*, inside this chromosomal region have been associated with cleft palate in mice (He et al., 2010; Rivera et al., 2009), but targeted sequencing of all exons and exon-intron boundaries of these two genes did not find any mutation in the *ENU1483* line.

Analysis of whole exome sequencing results revealed that the cleft palate pups were homozygous for novel single nucleotide changes in three closely linked genes within the Chromosome 16 region: a G-to-A transition at the intron-9 splice donor site in the *Golgb1* gene (*Golgb1*$^{ivs9+1G>A}$), a C-to-T transition that causes a S793F missense mutation in the *Itgb5* gene (*Itgb5*^{S793F}), and a G-to-A transition that causes a G179S missense mutation in the *Adcy5* gene (*Adcy5*^{G179S}) (Supplementary Table 2). Genomic PCR followed by Sanger sequencing confirmed that all three mutations were ENU-induced and absent in the parental A/J and FVB/NJ strains. Since neither *Itgb5* null mice nor *Adcy5* null mice have palate defects (Huang et al., 2000; Iwamoto et al., 2003) and since *ocd/ocd* rats exhibit syndromic cleft palate associated with a *Golgb1* disruption (Katayama et al., 2011), the *Golgb1*$^{ivs9+1G>A}$ mutation became a prime candidate for causing cleft palate in the *ENU1483* mice.

The *ENU1483* mutant mice exhibit aberrant *Golgb1* mRNA splicing and loss of Golgb1 protein

The *Golgb1* gene contains 22 exons, with the ATG start codon located in exon-2 (Fig. 1A). We performed RT-PCR using two different pairs of primers flanking exon-9 and exon-10 sequences and found that the *ENU1483* mutant tissues yielded larger PCR fragments than the wildtype samples (Fig. 1B). Sequencing the RT-PCR products revealed that the mutant *Golgb1*

mRNAs contained extra 435 nucleotides from the 5' region of intron-9, indicating splicing of the mutant *Golgb1* pre-mRNAs from a cryptic splice donor site inside intron-9 (Fig. 1A).

The mutant *Golgb1* mRNAs contain an in-frame stop codon just 20 nucleotides 3' to the disrupted splice site (Fig. 1A). Western blot analysis using a polyclonal antibody against the N-terminal 469 residues of human GOLGB1 protein (Abcam ab24586) detected Golgb1 protein specifically in the wildtype samples but no product in the homozygous mutant embryos (Fig. 1C). Immunofluorescent staining also showed absence of Golgb1 protein in the homozygous mutant embryos (Fig. 2A-F) although the mutant cells appear to have intact Golgi apparatus, as marked by localized staining of another well-known Golgi marker GM130 (Nakamura et al., 1995) (Fig. 2A-F).

We further performed transmission electron microscopy (TEM) analysis and found that the *Golgb1*$^{ivs9+1G>A}$ homozygous mutant embryonic palate cells had normal looking Golgi structures (Fig. 2G, H). These data are consistent with previous reports from Golgb1 (giantin) knockdown studies in tissue culture cells that Golgb1 is not required for Golgi structural integrity (Petrosyan et al., 2012; Petrosyan et al., 2014; Puthenveedu and Linstedt, 2001; Wong and Munro, 2014).

Loss of Golgb1 function causes cleft palate in mice

To validate that the cleft palate defect was due to loss of Golgb1 function, we first purchased target-verified mouse embryonic stem (ES) cell clones containing the "knockout-first and conditional ready" *Golgb1*$^{tm1a(EUCOMM)}$ gene-targeted allele from the International Knockout Mouse Consortium and generated high percentage chimeric founder male mice through blastocyst microinjection. However, none of the chimeric mice gave germ line transmission of the correctly targeted *Golgb1*$^{tm1a(EUCOMM)}$ allele. Recently, the RNA-guided, nuclease-mediated genome editing technology, based on the Archaeal type II CRISPR (clustered regularly interspaced short palindromic repeat)/Cas9 system, has been successfully adapted for genome editing in mammals (Jinek et al., 2012; Mali et al., 2013; Ran et al., 2013; Wang et al., 2013). We thus used the CRISPR/Cas9 system to create independent *Golgb1* mutant alleles in mice. We designed synthetic guide RNAs (sgRNAs) to target exon-10 and exon-13 regions, respectively, of the *Golgb1* gene (Fig. 3A) and tested the sgRNA/Cas9 constructs by transfection of mouse kidney MK4 cells. SURVEYOR assay of the transfected cells showed that the E13-1 and E10

sgRNAs resulted in highly efficient editing of the target sites (Fig. 3B). The E13-1 and E10 sgRNAs were subsequently co-injected with *Cas9* mRNAs into FVB/NJ zygotes for generation of *Golgb1* mutant mice. Of 34 founder mice, 9 carried various indel mutations that cause frame shift in either exon-10 or exon-13 (Fig. 3C). In addition, one founder mouse carrying an 11 kb deletion from exon-10 to exon-13, resulting in an in-frame deletion of 137 amino acid residues in the protein product, was obtained (Fig. 3C). We crossed the founder mice to FVB/NJ wildtype mice and obtained germ-line transmission of five distinct *Golgb1* alleles. F1 male mice carrying four distinct alleles (one exon-10 indel and three exon-13 indel mutations), respectively, were crossed to *Golgb1*$^{ivs9+1G>A}$ heterozygous female mice and embryos harvested at E16.5 to E18.5 for phenotypic analysis. All trans-heterozygous embryos had cleft palate (Fig. 4B, D).

We next generated and analyzed embryos homozygous for a frame-shift indel mutation in exon-10 as well as those homozygous for each of two exon-13 mutations that deleted 41 bp and 25 bp, respectively. Immunofluorescent staining of E13.5 homozygous embryos confirmed absence of the Golgb1 protein in these mutants (Fig. 4F). Histological analysis at E15.5 and E16.5, respectively, showed that the homozygous mutants had cleft palate (Fig. 5F, H). These results confirm that loss of *Golgb1* function causes cleft palate in mice. Mice homozygous for the 11kb deletion from exon-10 to exon-13 survived postnatally and appeared grossly normal, indicating that the in-frame deletion of 137 amino acid residues in the cytoplasmic domain of the Golgb1 protein did not significantly disrupt its cellular function.

Loss of Golgb1 function disrupted palatal shelf elevation

To investigate the mechanism of cleft palate pathogenesis in *Golgb1* mutant mice, we performed histological analysis of *Golgb1*$^{ivs9+1G>A}$, *Golgb1*$^{E13\text{-}25bp}$, and *Golgb1*$^{E13\text{-}41bp}$ homozygous mutant embryos, respectively, and their control littermates from E12.5 to P0. The palatal shelves appeared similar in shape and size in the *Golgb1* mutant and control littermates up to E13 (Fig. 5A, B). By E14.5, however, when the palatal shelves had already elevated and initiated fusion at the midline in wildtype and heterozygous embryos, the palatal shelves in homozygous mutant embryos remained vertically oriented (Fig. 5C, D). From E15.5 to E16.5, wildtype and heterozygous embryos showed extensive fusion of the palatal shelves throughout the anterior-posterior axis (Fig. 5E, G), but homozygous mutant embryos still had separate, vertically oriented, palatal shelves (Fig. 5F, H). In addition, the tongue did not descend to the

floor of the oral cavity in the mutant embryos (Fig. 5D, F, H).

Since Golgb1 is ubiquitously expressed, we examined whether the *Golgb1* mutant embryos have defects in early neural crest development. We carried out lineage tracing of migrating neural crest cells by using the *Wnt1Cre*:*R26R* genetic lineage labeling system (Chai et al., 2000; Jiang et al., 2000) and examined distribution of neural crest derived cells from E9.5 to E12.5 in the *Golgb1*$^{ivs9+1G>A}$ homozygous mutant and control littermates. No differences in the patterns of labeled neural crest cells were detected in the *Golgb1*$^{ivs9+1G>A}$ homozygous mutant and control littermates (Supplementary Fig. 2).

We analyzed whether *Golgb1* mutant embryos had defects in palatal cell proliferation. No significant differences in the percentage of BrdU-labeled cells in the palatal epithelium or mesenchyme were detected in the *Golgb1*$^{ivs9+1G>A}$ homozygous mutant and control littermates at E12.5 and E13.5, respectively (Supplementary Fig. 3).

Although palatal cell proliferation index was not significantly different between the mutant and control embryos, careful examination of histological sections of embryos after E13.5, but prior to palatal shelf elevation, showed that the mutant palatal shelves became consistently smaller, but with higher cellular density, than those in the control littermates. Quantification of DAPI-stained nuclei on serial sections of the embryos revealed that the mutant palatal shelves had significantly increased cellular density throughout the anterior-posterior axis prior to palatal shelf elevation (Fig. 6C). Including alcian blue staining in the histology procedure showed that the intensity of alcian blue staining is obviously reduced in the mutant palatal mesenchyme in comparison with wildtype littermates (Fig. 6A, B), suggesting that the mutant palatal mesenchyme cells have a defect in synthesis or accumulation of polysaccharides such as glycosaminoglycans (GAGs).

Hyaluronan (HA) is a high molecular mass GAG in the palatal mesenchyme extracellular matrix (ECM) implicated in playing a role in palatal shelf elevation (Brinkley and Bookstein, 1986; Ferguson, 1988). Detection of HA using biotin-labeled HA-binding peptide (HABP) revealed that *Golgb1* mutant embryos have significantly reduced HA accumulation throughout the anterior-posterior axis of the palatal mesenchyme, in comparison with control littermates, at E13.5 (Fig. 7). Similar to the alcian blue staining pattern, HA appears to accumulate at higher levels in the nasal side and in the hinge region of the palatal mesenchyme in the control embryos, and HA accumulation in both regions was reduced in the mutant embryos. Since HA is a major

component of the palatal mesenchyme ECM, the dramatic reduction in HA accumulation is likely at least part of the reason for the increased cell density and slower volume expansion of the palatal mesenchyme in the *Golgb1* mutant embryos.

Although the reduced HA accumulation in the palatal mesenchyme indicates an intrinsic defect in the palatal shelf, it is possible that the failure of palatal shelf elevation in *Golgb1* mutant embryos might be secondary to failure of the tongue to descend. To investigate this possibility, we isolated E13.5 embryos from intercrosses of *Golgb1*$^{E13\text{-}25bp}$ and *Golgb1*$^{E13\text{-}41bp}$ heterozygous mice, respectively, and cultured freshly microdissected maxillary explants in suspension culture in modified BGJb medium for three days as described previously (Abbott, 2000; Shiota et al., 1990; Takahara et al., 2004). Of 8 litters of embryos, 8 embryos were homozygous mutants and all 8 mutant explants showed vertically oriented palatal shelves at the end of the 3-day culture (n=8, Fig. 8 B, D). In contrast, of the 43 wildtype and heterozygous explants from these litters, all showed horizontally oriented palatal shelves and 33 of them (77%) showed at least partial fusion of the palatal shelves at the midline (Fig. 8A, C). These results indicate that Golgb1 plays an intrinsic role in the palatal mesenchyme in regulating palatal shelf elevation.

Defects in protein glycosylation in the *Golgb1* mutant palatal mesenchyme

Whereas Golgi is the major site for GAG synthesis, HA is a unique GAG that is primarily synthesized at the plasma membrane (Fraser et al., 1997). However, HA synthases are integral membrane proteins synthesized in the endoplasmic reticulum (ER) and transported to the plasma membrane through the Golgi. We thus examined whether *Golgb1*$^{ivs9+1G>A}$ homozygous mutant palatal mesenchyme cells (MEPM) have defects in vesicle trafficking through the ER-Golgi secretory pathway using adenovirus expressing a GFP-tagged temperature-sensitive mutant of the vesicular stomatitis protein, VSVG^{ts045}-GFP. This mutant protein is unfolded and retained in the ER at 40 ^{o}C but it can fold properly and transit through the Golgi network at 32 ^{o}C. After incubating the infected cells at 40.5 ^{o}C for 20 hours, all VSVG^{ts045}-GFP molecules were retained in the ER in both control and *Golgb1*$^{ivs9+1G>A}$ homozygous mutant MEPM cells (Supplementary Fig. 4). After transferring the infected cells to 32^{o}C for 20 minutes, the VSVG^{ts045}-GFP proteins were localized in the Golgi network (Supplementary Fig. 4). No differences in the patterns of VSVG^{ts045}-GFP protein localization were detected in between the control and *Golgb1*$^{ivs9+1G>A}$

homozygous mutant cells, suggesting that Golgb1 function is not required for anterograde trafficking from ER through the Golgi.

It has been shown that HA synthase activity is regulated by protein glycosylation (Vigetti et al., 2009). To investigate whether protein glycosylation is affected during palate development in *Golgb1* mutant embryos, we examined patterns of binding by GSII Lectin from *Griffonia simplicifolia*, which preferentially binds to terminal nonreducing N-acetyl-D-glucosamine, a glycan structure expected to be rare in properly modified mature glycoproteins (Puthenveedu et al., 2006; Smits et al., 2010). As shown in Fig. 9, most palatal mesenchyme cells in the control embryos did not have much GSII Lectin binding (Fig. 9A, C, E), but *Golgb1* mutant palatal mesenchyme cells, particularly in the middle and posterior regions of the palatal shelves, exhibited increased GSII Lectin binding (Fig. 9D, F, G). The palatal regions that exhibit increased GSII binding in the mutant embryos appear to partly overlap with the regions that exhibited reduced HA accumulation, including proximal palatal mesenchyme at the nasal side and the hinge regions of the palatal shelves (compare Fig. 8C-G with Fig. 9C-G).

To further investigate the effect of loss of Golgb1 function on protein glycosylation during palate development, we tested the Vector Lectin Kit III (Vector, cat # BK 3000), which contains multiple lectins with selectivity for distinct glycosylation products, for differential binding to the palatal tissues in the *Golgb1* mutant and control littermates. We found that *Golgb1* mutant palatal mesenchyme had significantly increased binding to both peanut agglutinin (PNA) and *Vicia villosa* agglutinin (VVA). PNA, isolated from *Arachis hypogaea* (peanut), has high specificity for terminal β-galactose residues of glycoproteins (Pereira et al., 1976; Soga et al., 2015). In most mature glycoproteins, the β-galactose residues are further modified by sialylation (Gillespie et al., 1993). Thus, PNA binds to a broad range of cell surface glycoproteins following treatment with neuraminidase (sialidase) to remove terminal sialic acids (Novogrodsky et al., 1975). We found that neuraminidase treatment of sections of E13.5 wildtype embryos resulted in strong binding of the palatal mesenchyme to PNA (Fig. 10A, C, E), indicating that palatal mesenchyme cells normally produce a large amount of sialylated glycoproteins. Whereas the neuraminidase-treated sections of E13.5 mutant palatal shelves exhibited increased PNA binding compared to that in control littermates, particularly in the middle and posterior regions (Fig. 10B, D, F, G), the untreated mutant palatal mesenchyme also exhibited significant binding to PNA whereas little PNA binding was detected in the untreated wildtype palatal mesenchyme (Fig. 10A'-F').

Quantification of the mean fluorescence intensity in the palatal mesenchyme on serial sections showed that PNA binding is significantly increased throughout the anterior-posterior axis of the developing palatal shelves of the mutant embryos in comparison with control littermates (Fig. 10G'). VVA, isolated from *Vicia villosa* (hairy vetch) seeds, binds highly selectively to the Tn antigen, a simple monosaccharide structure composed of N-acetyl-D-galactosamine with a glycosidic α linkage to serine/threonine residues in glycoproteins (Ju et al., 2011; Tollefsen and Kornfeld, 1983). Tn antigen is produced at the first step of mucin-type O-glycosylation in the cis-Golgi and is usually further modified by sialylation or addition of additional sugar residues (Ju et al., 2011). We found that *Golgb1* mutant embryos exhibit significantly increased VVA binding throughout the anterior-posterior axis of the palatal mesenchyme at E13.5, in comparison with control littermates (Fig. 11A-G). Following neuraminidase treatment, whereas sections of the wildtype E13.5 embryonic heads exhibited low VVA binding to the palatal mesenchyme, sections of the mutant palatal shelves exhibited significantly stronger VVA binding to palatal mesenchyme (Fig. 11A'-G'). Together, these results indicate that *Golgb1* mutant embryos have defects at multiple steps in protein glycosylation during palate development. Remarkably, both PNA and VVA showed preferential binding to the nasal side of the palatal mesenchyme in the mutant embryos (Figs. 10 - 11) whereas PNA binding to the neuraminidase-treated samples showed relatively uniform distribution throughout the palatal mesenchyme in both control and mutant embryos (Fig. 10), suggesting that Golgb1 is required for proper glycosylation of only a subset of glycoproteins that are preferentially synthesized in the nasal side palatal mesenchyme.

Discussion

Most of our current knowledge regarding the cellular and molecular mechanisms of mammalian organogenesis has arisen through "reverse genetic" approaches in which the gene of interest is mutated and the phenotype analyzed. However, reverse genetic approaches are inevitably biased toward studying genes with some prior information that suggests a detectable mutant phenotype. To circumvent the limitations of these approaches, several large-scale random mutagenesis screens have been performed in mice using both chemical and genetic mutagens (Araki et al., 2009; Barbaric et al., 2007; Boles et al., 2009; Hrabe de Angelis and Strivens, 2001; Sakuraba et al., 2005). Recent advances in genomic sequencing technologies have enabled rapid identification of mutations by using exome or whole genome sequencing (Caruana et al., 2013). Because of the high rate of ENU-induced mutations throughout the genome, however, there are almost always multiple linked nucleotide changes around each candidate gene and it is critical to validate candidate causal genes by generation and analysis of independent mutant mouse lines. In this study, we used ENU mutagenesis to isolate a new cleft palate mutation and SNP mapping and exome sequencing to identify the candidate causal mutation, followed by validating the requirement for Golgb1 function in palate development through generation of mice carrying independent mutant alleles using CRISPR/Cas9 genome editing. Despite several other ENU mutagenesis screens designed to identify recessive mutations affecting embryogenesis, no *Golgb1* mutant mice have been reported. Thus, combining phenotype-driven mutation discovery with validation of causality using CRISPR/Cas9-mediated genome editing is an effective approach for uncovering novel molecular mechanisms underlying structural birth defects and other biological processes.

Golgb1 is not required for Golgi structural integrity but rather plays critical roles in tissue morphogenesis including palatal shelf elevation

Golgb1 belongs to the golgin family of large coiled-coil proteins located at the cytoplasmic surface of the Golgi apparatus (Munro, 2011). Of all golgins, Golgb1 is unique because it contains a transmembrane domain at its C-terminus, which anchors the protein to the Golgi membrane or COPI vesicles, and a p115-binding domain at its N-terminus (Alvarez et al., 2001; Puthenveedu and Linstedt, 2001; Sapperstein et al., 1995; Sonnichsen et al., 1998). This unique structure suggested that it might play a role in vesicle tethering to the Golgi membranes

in conjunction with p115 and GM130, another p115-interacting golgin (Alvarez et al., 2001; Lesa et al., 2000; Linstedt et al., 2000; Sonnichsen et al., 1998). Whereas several other golgins, as well as p115, have been shown to be essential for Golgi structural integrity in siRNA knockdown studies in cell culture assays, knockdown of either *Golgb1* mRNAs or protein did not cause disruption of Golgi structures or reassembly following mitosis (Koreishi et al., 2013; Puthenveedu and Linstedt, 2001). Recently, Kim et al. generated mice heterozygous for *Uso1*, encoding the p115 protein, and confirmed genetically that p115 function is required for Golgi structural integrity and cell survival (Kim et al., 2012). On the other hand, rats homozygous for a frame-shift mutation in *Golgb1* survive to birth (Katayama et al., 2011), indicating that Golgb1 is not essential for cell survival *in vivo*. Our finding that mice homozygous for either the ENU-induced splicing mutation or the CRISPR/Cas9-induced frame-shift mutations also survive to birth further validates this conclusion.

We found that mouse embryos deficient in Golgb1 consistently exhibit failure of palatal shelf elevation. Although failure of palatal shelf elevation has been described in several other mutant mouse strains (Jiang et al., 1998; Jin et al., 2010; Lan et al., 2004; Matsumura et al., 2011; Snyder-Warwick et al., 2010; Yu et al., 2010), the molecular and cellular mechanisms regulating palate shelf elevation are still not well understood (Bush and Jiang, 2012; Ferguson, 1988). It has been proposed that an intrinsic force is progressively generated to drive palatal shelf elevation and the chief component of this intrinsic force appears to be regionally specific accumulation of extracellular GAGs, predominantly HA (Ferguson, 1988). HA is capable of binding a large amount of water and HA accumulation results in swelling of the ECM and a corresponding decrease in cell density (Brinkley and Bookstein, 1986; Ferguson, 1988). Brinkley and Vickerman showed that reducing HA in palatal mesenchyme through pharmacological enhancement of its degradation inhibited palatal shelf elevation in organ culture as well as in vivo (Brinkley and Vickerman, 1982). Palatal shelf elevation defect in mice homozygous for the *Fgfr2*^{C342Y} missense mutation was also associated with reduced HA accumulation in the palatal mesenchyme (Snyder-Warwick et al., 2010). We found that *Golgb1* mutant embryos exhibit reduced HA accumulation and concomitantly increased cell density in the palatal mesenchyme by E13.5. Kikukawa et al. showed that the *ocd/ocd* neonatal rats had drastically reduced amounts of HA in the cartilage than control littermates (Kikukawa, 1990). Thus, Golgb1 plays a critical role in HA accumulation in multiple tissues and reduction in HA accumulation in the

palatal mesenchyme is likely an important factor in the pathogenesis in *Golgb1* mutant mice.

Golgb1 plays an important role in protein glycosylation

Recent cell culture studies suggest that Golgb1 mediates Golgi-targeting of specific glycosyltransferases. In particular, siRNA knockdown studies suggest that the C2GnT-M and C2GnT-L synthases in the O-glycosylation pathway use Golgb1 exclusively to target to Golgi membrane whereas C1GalT1 and ST3Gal1 synthases use Golgb1 and GM130-GRASP65 as alternative docking sites (Petrosyan et al., 2012; Petrosyan et al., 2014; Wong and Munro, 2014). O-glycosylation in the Golgi starts with synthesis of the glycoconjugate GalNAc-a1-O-Ser/Thr, known as the Tn antigen. The most common modification of the Tn antigen is catalyzed by the core 1 β1,3-galatosyltransferase (C1GalT1) to produce the Core 1 disaccharide known as the T antigen (Ju et al., 2011). Remarkably, we found that *Golgb1* mutant palatal mesenchyme cells exhibit significantly increased binding to both Tn and T antigen-binding lectins, VVA and PNA, respectively. These results are consistent with the cell biological data that Golgb1 is involved in Golgi targeting of the core1 and core2 glycosyltransferases and identify an important role for Golgb1 in regulating the early steps of O-glycosylation during mammalian organogenesis.

Mice lacking another ubiquitously expressed member of the golgin family, GMAP-210, encoded by the *Trip11* gene, die neonatally with skeletal dysplasia (Smits et al., 2010). Human patients homozygous for loss-of-function mutations in GMAP-210 also exhibit neonatal lethal skeletal dysplasia (Smits et al., 2010). Although *Trip11* mutant mouse skin fibroblasts and chondrocytes showed impairment in protein glycosylation, no cleft palate phenotype has been noted in *Trip11* null mice, indicating that GMAP-210 and Golgb1 have distinct cellular functions. Further comparative investigation of the distinct and complementary functions of Golgb1, GMAP-210, and other members of the golgin family in protein glycosylation and tissue morphogenesis in mutant mouse models will provide novel insights into the cellular and molecular mechanisms involving Golgi-associated proteins in human diseases.

Materials and Methods

ENU mutagenesis screening, genetic mapping, and whole exome sequencing analysis

All animal studies were performed in accordance with the guidelines set by the Institutional Animal Care and Use Committee (IACUC) at the Cincinnati Children's hospital Medical Center. ENU mutagenesis screening was conducted as described previously (Coles and Ackerman, 2013). One line exhibiting autosomal recessive inheritance of isolated cleft palate, *ENU1483*, was established and maintained by backcrossing the carrier male to FVB/NJ female mice. Genomic DNA from seventeen cleft palate pups from this line was used for linkage mapping using the mouse universal genotyping array (MUGA) SNP microarray (GeneSeek, Inc., Lincoln, NE), which resulted in mapping the cleft palate mutation to proximal Chromosome 16.

Whole exome sequencing and variant calling were conducted at the Cincinnati Children's Hospital Medical Center DNA Core Facility. Novel variants in the mapped Chromosome 16 region were verified by genomic PCR and Sanger sequencing.

RT-PCR analysis of the effect of the *Golgb1*$^{ivs9+1>1A}$ mutation

The PCR primers Golgb1RT-1F (5'-GTAGGATCCTGCTGCAGAAGGAGCTAACG-3') and Golgb1RT-2R (5'-GATGGATCCAGAGCTAAGGAGCAAGG-3') were used to amplify a fragment of 704 bp from exon-8 to exon-11. Another forward primer Golgb1RT-3F (5'-AAGGTCGACCTGGAGACACAGTACAGT-3') was used in combination with Golgb1RT-2R to amplify a fragment of 405 bp from exon-9 to exon-11. RT-PCR products were gel-purified and sequenced by using the Sanger method.

Generation of *Golgb1* mutant mice using CRISPR/Cas9-mediated genome editing

We constructed one guide RNA (sgRNA) targeting exon-10 (target sequence 5'-GTCGCCCTCATTATTAACATC-3') and three sgRNAs targeting exon-13 (target sequences exon13-1: 5'-GCTGCACTTCTCTACGGTCG-3', exon13-2: 5'-CACCGCTGGTACTACTCTGCTCAAC-3', and exon13-3: 5'-CACCGCTGCAGGGCAAGAGGCCCGA-3') by using the online CRISPR Design Tool (http://crispr.mit.edu). The target sequences were subcloned into the PX459 mammalian Cas9-expression vector (Addgene #48139) and tested by transfection into cultured immortalized mouse embryonic kidney (MK4) cells (Ran et al., 2013; Valerius et al., 2002). MK4 cells were

provided by Dr. Steven Potter at Cincinnati Children's Hospital Medical Center from the original stock. A previously reported sgRNA for targeting the *Tet2* gene was used as positive control (Wang et al., 2013). The targeting efficiencies were estimated using SURVEYOR assays (Transgenomics). Subsequently, sgRNAs targeting exon-10 and exon-13, respectively, were synthesized *in vitro* and co-injected with *Cas9* mRNAs into zygotes from FVB/NJ inbred mice to generate gene-targeted mice in the CCHMC Transgenic Animal and Genome Editing Facility. Transgenic founder mice were identified by sequencing PCR products and bred to FVB/NJ inbred mice to test for germ-line transmission. G1 mice heterozygous for indel mutations that cause frame-shift in exon-10 or exon-13 of the *Golgb1* gene were crossed to the *Golgb1*$^{ivs9+1G>A}$ heterozygous mice to generate trans-heterozygotes or intercrossed to analyze phenotypes of homozygotes.

Immunofluorescent staining and Transmission Electron Microscopy (TEM)

Immunofluorescent staining was performed using paraffin or frozen sections following standard protocols (Xu et al., 2014). Primary antibodies used include rabbit anti-giantin (Abcam ab24586; lot # GR6988-3; 1:300), mouse anti-GM130 (BD610822; lot # 29000; 1:500), rabbit anti-ERGIC-53 (Sigma E1031; 1:250). For detection of HA, biotin-labeled HABP (Millipore 385911-50UG; lot# D00175939; 1:200) staining was detected using Texas-red conjugated streptavidin (Vector, 1:200). For Lectin binding assays, Alexa-594 conjugated Lectin GSII (Life Technologies; 1:200), biotin-conjugated Lectin VVA (Vector 1:200), or fluorescein-conjugated PNA (Vector, 1:200) were used. Slides were mounted with ProLong® Diamond Antifade Mountant (ThermoFisher). Nuclear density and fluorescence intensity over the entire palatal shelf area were recorded and analyzed separately for the anterior, middle, and posterior regions of the palatal shelves using ImageJ (http://fiji.sc/Fiji). The statistical significance of the results was assessed using Student's *t*-test.

For TEM, embryos were dissected at E13.5. Palatal shelves and limbs of each embryo were fixed with 3% glutaraldehyde, washed with sodium cacodylate buffer, post-fixed with 1% OsO_4, processed through an ethanol gradient, washed in serial dilutions of plastic (Ladd Research, LX-112)/propylene oxide mixture, and moved to 60°C for 3 days. The tissue samples were sectioned at 100 nm thickness using a Leica EM UC7 ultramicrotome and put onto 200-mesh copper grids for examination under a Hitachi Model 7650 transmission electron

microscope (EM Core of CCHMC).

Histology, western blotting, cell proliferation analysis and skeletal preparations

Embryos were dissected at desired stages (noon of date of vaginal plug detection was counted as day 0.5), processed for histology analysis as described (Baek et al., 2011; Xu et al., 2015).

For western blot assays, three pairs of micro-dissected palatal shelves (E14.0) were pooled and lysed in RIPA buffer containing proteinase inhibitors (Santa Cruz, SC-24948) and experiments repeated three times. The supernatant was mixed with Laemmli buffer and separated by SDS-PAGE on a 4-12% Mini-PROTEAN gel (Bio-Rad, Hercules, CA). Western blots were incubated with rabbit anti-giantin (Abcam ab24586, 1: 3,000) or anti-β-actin (Santa Cruz SC-47778, lot # 10710; 1:3,000) antibody followed by washing and incubation with HRP-conjugated secondary antibody. The signals were detected using Immobilon Western HRP peroxidase solution and Luminol reagent (EMD Millipore, Billerica, MA) and exposed to X-ray film (Associated Metals, Ann Arbor, MI).

Palatal cell proliferation was analyzed as described previously (Lan et al., 2004; Xu et al., 2015; Zhou et al., 2013). The numbers of BrdU-labeled nuclei and total nuclei were recorded for five independent control and mutant littermate pairs. Student's *t*-test was used to analyze the differences in the datasets and *p value less tha* 0.05 was considered statistically significant.

Skeletal preparations of E18 and P0 pups were performed as described previously (Liu et al., 2013; Zhou et al., 2013).

Roller bottle culture of embryonic maxillary explants

Freshly dissected maxillary explants of E13.5 embryos were cultured as described previously (Abbott, 2000; Shiota et al., 1990; Takahara et al., 2004). Briefly, 3 to 5 explants were placed in a 50 ml penicillin bottle with 8 ml BGJb medium (Invitrogen) supplemented with 2.8 mg/ml L-Glutamine, 6 mg/ml BSA and 1% penicillin and streptomycin. The bottle was flushed for 2 min each day with a gas mixture (50% O_2, 45% N_2 and 5% CO_2), sealed air-tight, and incubated at 37ºC on a Wheaton Mini Bench-Top roller bottle system at a speed of 25 rpm for three days. A small piece of tissue was taken from each explant for genotyping and explants were fixed individually for histological analyses.

Mouse embryonic palatal mesenchyme cell (MEPM) culture, and VSVG^{ts045}-GFP transfection

Palatal shelves were dissected from each E13.5 mouse embryo, rinsed in cold PBS, transferred into a 12-well tissue culture plate, and treated with 0.5% trypsin and 2.5% pancreatin in ice-cold PBS for 30 min to remove the epithelium. The palatal mesenchyme tissues were then treated with 0.5% trypsin/EDTA for 10 min at 37ºC, with pipetting up and down several times every 3 - 4 minutes to break into cell suspension, followed by culturing at 37ºC in DMEM supplemented with 10% FBS (Invitrogen) and 1% penicillin and streptomycin . Two hours later, the culture wells were rinsed with PBS to remove unattached cells and tissue debris, and replaced with fresh medium. Upon about 70% confluence, cells were trypsinized and split at 1:3 into 6-well tissue culture plates. Cells were cryopreserved upon 80% confluence.

VSVG^{ts045}-GFP adenovirus was provided by Dr. Yanzhuang Wang at University of Michigan (Xiang et al., 2013). Wildtype and mutant primary MEPM cells were plated, respectively, in slide chambers at a density of 2 x 10^6 cells/chamber. VSVG^{ts045}-GFP adenovirus was added at 0, 2.5x10^8, 5 x 10^8, and 10 x 10^8 particles per chamber, respectively, and incubated at 40.5 ºC (5% CO2) for 20 hours and shifted to 32ºC (5% CO2) for fixation at 0, 20, and 60 minutes, respectively, after the temperature shift. The cells were co-immunostained for ERGIC-53 (Sigma E1031, 1:250) and GM130 (BD610822, lot # 29000,1:500).

Acknowledgments

We thank Dr. Yanzhuang Wang for providing the VSVG^{ts045}-GFP adenovirus. We thank Cai Zhang and Takahisa Nakamura for help with adenovirus preparation, and Julie Serr and Lynessa McGee for laboratory assistance. This work was supported by Cincinnati Children's Hospital Medical Center Trustee Award (YL) and by National Institutes of Health National Institute of Dental and Craniofacial Research grants R03DE023864 (YL) and R01DE013681 (RJ).

Reference

Abbott, B.D., 2000. Palatal dysmorphogenesis. Palate organ culture. Methods Mol Biol 136, 195-201.

Alvarez, C., Garcia- Mata, R., Hauri, H.O., Sztul, E., 2001. The p115-interactive Proteins GM130 and Giantin Participate in Endoplasmic Reticulum-Golgi Traffic. J Biol Chem. 276, 2693-2700.

Araki, M., Araki , K., Yamamura, K., 2009. International gene trap project: towards gene-driven saturation mutagenesis in mice. Curr. Pharm. Biotechnol. 10, 221-229.

Baek, J.A., Lan, Y., Liu, H., Maltby, K.M., Mishina, Y., Jiang, R., 2011. Bmpr1a signaling plays critical roles in palatal shelf growth and palatal bone formation. Dev Biol 350, 520-531.

Barbaric, Wells, S., Russ, A., Dear, T.N., 2007. Spectrum of ENU-induced mutations in phenotype-driven and gene-driven screens in the mouse. Environ. Mol. Mutagen 48, 124-142.

Boles , M.K., Wilkinson , B.M., Wilming, L.G., Liu, B., Probst, F.J., Harrow, J., Grafham, D., Hentges, K.E., Woodward, L.P., Maxwell, A., Mitchell, K., Risley, M.D., Johnson, R., Justice, M.J., 2009. Discovery of candidate disease genes in ENU-induced mouse mutants by large-scale sequencing, including a splice-site mutation in nucleoredoxin. Plos Genet 5:e1000759.

Brinkley, L., Vickerman, M., 1982. The effects of chlorcyclizine-induced alterations of glycosaminoglycans on mouse palatal shelf elevation in vivo and in vitro. J. Embryol. exp. morph 69, 193-213.

Brinkley, L.L., Bookstein, F.L., 1986. Cell distribution during mouse secondary palate closure. II. Mesenchymal cells. J Embryol Exp Morphol 96, 111-130.

Bush, J.O., Jiang, R., 2012. Palatogenesis: morphogenetic and molecular mechanisms of secondary palate development. Development 139, 231-243.

Cao, X., Ballew, N., Barlowe, C., 1998. Initial docking of ER-derived vesicles requires Uso1p and Ypt1p but is independent of SNARE proteins. EMBO J 17, 2156-2165.

Caruana, G., Farlie, P.G., Hart, A.H.B.-F., S., Wallace, M.J., Dobbie MS, G., C.T., Miller , K.A., Whittle, B., Abud, H.E., Arkell, R.M., Cole , T.J., Harley, V.R., Smyth, I.M., Bertram, J.F., 2013. Genome-wide ENU mutagenesis in combination with high density SNA analysis and exome sequencing provides rapid identification of novel mouse models of developmental disease. PLoS One 8:e55429.

Chai, Y., Jiang, X., Ito, Y., Bringas, P., Jr., Han, J., Rowitch, D.H., Soriano, P., McMahon, A.P., Sucov, H.M., 2000. Fate of the mammalian cranial neural crest during tooth and mandibular morphogenesis. Development 127, 1671-1679.

Coles, G.L., Ackerman, K.G., 2013. Kif7 is required for the patterning and differentiation of the diaphragm in a model of syndromic congenital diaphragmatic hernia. Proc Natl Acad Sci U S A 110, E1898-1905.

Ferguson, M.W., 1988. Palate development. Development 103 Suppl, 41-60.

Follit, J.A., San Agustin, J.T., Xu, F., Jonassen, J.A., Samtani, R., Lo, C.W., Pazour, G.J., 2008. The Golgin GMAP210/TRIP11 anchors IFT20 to the Golgi complex. PLoS Genet 4, e1000315.

Fraser, J.R.E., Laurent, T.C., Laurent, U.B.G., 1997. Hyaluronon: its nature, distribution, functions and turnover. Journal of Internal Medicine.

Freeze, H.H., Ng, B.G., 2011. Golgi glycosylation and human inherited diseases. Cold Spring Harb Perspect Biol 3, a005371.

Gillespie, W., Paulson, J.C., Kelm, S., Pang, M., Baum., L.G., 1993. Regulation of a-2,3-sialyltransferase expression correlates with conversion of peanut agglutinin (PNA)+ to PNA- phenotype in developing thymocytes. j. Biol. Chem 268, 3802-3804.
Gritli-Linde, A., 2007. Molecular control of secondary palate development. Dev Biol 301, 309-326.
He, F., Popkie, A.P., Xiong, W., Li, L., Wang, Y., Phiel , C.J., Chen, Y., 2010. Gsk3beta is required in the epithelium for palatal elevation in mice. Dev. Dyn 239, 3235-3246.
Hilliard, S.A., Yu, L., Gu, S., Zhang, Z., Chen, Y.P., 2005. Regional regulation of palatal growth and patterning along the anterior-posterior axis in mice. J Anat 207, 655-667.
Hrabe de Angelis, M., Strivens, M., 2001. Large-scale production of mouse phenotypes: the search for animal models for inherited diseases in humans. Brief Bioinform 2, 170-180.
Huang, X., Griffiths, M., Wu, J., Farese, R.V., Sheppard, D., 2000. Normal development, wound healing, and adenovirus susceptibility in beta5-deficient mice. Mol Cell Biol 20, 755-759.
Iwamoto, T., Okumura, S., Iwatsubo, K., Kawabe, J., Ohtsu, K., Sakai, I., Hashimoto, Y., Izumitani, A., Sango, K., Ajiki, K., Toya, Y., Umemura, S., Goshima, Y., Arai, N., Vatner, S.F., Ishikawa, Y., 2003. Motor dysfunction in type 5 adenylyl cyclase-null mice. J Biol Chem 278, 16936-16940.
Jiang, R., Lan, Y., Chapman, H., Shawber, C., Norton, C., Serreze, D., Weinmaster, G., Gridley, T., 1998. Defects in limb, craniofacial, and thymic development in Jagged2 mutant mice. Genes Dev 12, 1046–1057.
Jiang, X., Rowitch, D.H., Soriano, P., McMahon, A.P., Sucov, H.M., 2000. Fate of the mammalian cardiac neural crest. development 127, 16-17-1616.
Jin, J.Z., Tan, M., Warner, D.R., Darling, D.S., Higashi, Y., Gridley, T., Ding, J., 2010. Mesenchymal cell remodeling during mouse secondary palate reorientation. Dev Dyn 239, 2110-2117.
Jinek, M., Chylinski, K., Fonfara, I., Hauer, M., Doudna, J.A., Charpentier, E., 2012. A programmable dual-RNA-guided DNA endonuclease in adaptive bacterial immunity. Science 337, 816-821.
Ju, T., Otto, V.I., Cummings, R.D., 2011. The Tn antigen-structural simplicity and biological complexity. Angew Chem Int Ed Engl 50, 1770-1791.
Katayama, K., Sasaki, T., Goto, S., Ogasawara, K., Maru, H., Suzuki, K., Suzuki, H., 2011. Insertional mutation in the Golgb1 gene is associated with osteochondrodysplasia and systemic edema in the OCD rat. Bone 49, 1027-1036.
Kikukawa, K., Kamei, T., Suzuki, K. and Maita, K., 1990. Electron microscopic observations and electrophoresis of the glycosaminoglycans in the epiphyseal cartilage of the congenital osteochondrodysplasia rat (ocd/ocd. Matrix 10, 378–387.
Kim, S., Hill, A., Warman, M.L., Smits, P., 2012. Golgi disruption and early embryonic lethality in mice lacking USO1. PLoS One 7, e50530.
Koreishi, M., Gniadek, T.J., Yu, S., Masuda, J., Honjo, Y., Satoh, A., 2013. The golgin tether giantin regulates the secretory pathway by controlling stack organization within Golgi apparatus. PLoS One 8, e59821.
Lan, Y., Ovitt, C.E., Cho, E.S., Maltby, K.M., Wang, Q., Jiang, R., 2004. Odd-skipped related 2 (Osr2) encodes a key intrinsic regulator of secondary palate growth and morphogenesis. Development 131, 3207-3216.
Lan, Y., Xu, J., Jiang, R., 2015. Cellular and Molecular Mechanisms of Palatogenesis, in: Chai, Y. (Ed.), Craniofacial Development. Elsevier.

Lesa, G.M., Seemann, J., Shorter, J., Vandekerckhove, J., J., W., 2000. The amino-terminal domain of the Golgi protein giantin interacts directly with the vesicle-tethering p115. J. Biol. Chem. 275, 2831–2836.
Linstedt, A.D., Hauri, H.P., 1993. Giantin, a novel conserved Golgi membrane protein containing a cytoplasmic domain of at least 350 kDa. Mol Biol Cell 4, 679-693.
Linstedt, A.D., Jesch, S.A., Mehta, A., Lee, T.H., Garcia-Mata, R., Nelson, D.S., Sztul, E., 2000. Binding relationships of membrane tethering components.The giantin N terminus and the GM130 N terminus compete for binding to the p115 C terminus. J. Bio Chem 275, 10196-10201.
Liu, H., Lan, Y., Xu, J., Chang, C.F., Brugmann, S.A., Jiang, R., 2013. Odd-skipped related-1 controls neural crest chondrogenesis during tongue development. Proc Natl Acad Sci U S A 110, 18555-18560.
Mali, P., Yang, L., Esvelt, K.M., Aach, J., Guell, M., DiCarlo, J.E., Norville, J.E., Church, G.M., 2013. RNA-guided human genome engineering via Cas9. Science 339, 823-826.
Matsumura, K., Taketomi, T., Yoshizaki, K., Arai, S., Sanui, T., Yoshiga, D., Yoshimura, A., Nakamura, S., 2011. Sprouty2 controls proliferation of palate mesenchymal cells via fibroblast growth factor signaling. Biochem Biophys Res Commun. 404, 1076-1082.
Mellman, I., Warren, G., 2000. The road taken: past and future foundations of membrane traffic. Cell 100, 99-112.
Moore, K.L., Persaud, T.V.N., 1998. Before We are Born: essentials of embryology and birth defects (5th ed). W. B. Saunders Company.
Munro, S., 2011. The golgin coiled-coil proteins of the Golgi apparatus. Cold Spring Harb Perspect Biol 3.
Nakamura, N., Rabouille, C., Watson, R., Nilsson, T., Hui, N., Slusarewicz, P., Kreis, T.E., Warren, G., 1995. Characterization of a cis-Gol Matrix Protein, GM130. J. Cell Biol. 131, 1715-1726.
Novogrodsky, A., Lotan, R., Ravid, A., Sharon, N., 1975. Peanut Agglutinin, A new mitogen that binds to galactosyl sites exposed after neuraminidase treatment. J Immunol 115, 1243-1248.
Pereira, M.A., Kabat, E.A., Lotan, R., Sharon, N., 1976. Immunochemical studies on the specificity of the peanut (Arachis hypogaea) agglutinin. Carbohydr. Res 51, 107-118.
Petrosyan, A., Ali, M.F., Cheng, P.W., 2012. Glycosyltransferase-specific Golgi-targeting mechanisms. J Biol Chem 287, 37621-37627.
Petrosyan, A., Holzapfel, M.S., Muirhead, D.E., Cheng, P.W., 2014. Restoration of compact Golgi morphology in advanced prostate cancer enhances susceptibility to galectin-1-induced apoptosis by modifying mucin O-glycan synthesis. Mol Cancer Res 12, 1704-1716.
Puthenveedu, M.A., Bachert, C., Puri, S., Lanni, F., Linstedt, A.D., 2006. GM130 and GRASP65-dependent lateral cisternal fusion allows uniform Golgi-enzyme distribution. Nat Cell Biol 8, 238-248.
Puthenveedu, M.A., Linstedt, A.D., 2001. Evidence that Golgi structure depends on a p115 activity that is independent of the vesicle tether components giantin and GM130. J Cell Biol 155, 227-238.
Ran, F.A., Hsu, P.D., Wright, J., Agarwala, V., Scott, D.A., Zhang, F., 2013. Genome engineering using the CRISPR-Cas9 system. Nat Protoc 8, 2281-2308.

Rivera, C., Yamben, I.F., Shatadal, S., Waldof, M., Robinson, M.L., Griep, A.E., 2009. Cell-autonomous requirements for Dlg-1 for lens epithelial cell structure and fiber cell morphogenesis. Dev Dyn 238, 2292-2308.
Sakuraba, Y., Sezutsu, H., Takahasi, K.R., Tsuchihashi, K., Ichikawa, R., Fujimoto, N., Kaneko, S., Nakai, Y., Uchiyama, M., Goda, N., Motoi, R., Ikeda, A., Karashima, Y., Inoue, M., Kaneda, H., Masuya, H., Minowa, O., Noguchi, H., Toyoda, A., Sakaki, Y., Wakana, S., Noda, T., Shiroishi, T., Gondo.Y., 2005. Molecular characterization of ENU mouse mutagenesis and archives. Biochem. Biophys. Res. Comm 336, 609-616.
Sapperstein, S.K., Walter, D.M., Grosvenor, A.R., Heuser, J.E., Waters, M.G., 1995. p115 is a general vesicular transport factor related to the yeast endoplasmic reticulum to Golgi transport factor Uso1p. Proc Natl Acad Sci U S A 92, 522-526.
Shiota, K., Kosazuma, T., Klug, S., Neubert, D., 1990. Development of the fetal mouse palate in suspension organ culture. Acta Anat (Basel) 137, 59-64.
Short, B., Haas, A., Barr, F.A., 2005. Golgins and GTPases, giving identity and structure to the Golgi apparatus. Biochim Biophys Acta 1744, 383-395.
Smits, P., Bolton, A.D., Funari, V., Hong, M., Boyden, E.D., Lu, L., Manning, D.K., Dwyer, N.D., Moran, J.L., Prysak, M., Merriman, B., Nelson, S.F., Bonafé, L., Superti-Furga, A., Ikegawa, S., Krakow, D., Cohn, D.H., Kirchhausen, T., Warman, M.L., Beier, D.R., 2010. Lethal skeletal dysplasia in mice and humans lacking the golgin GMAP-210. N Engl J Med 362, 206-216.
Snyder-Warwick, A.K., Perlyn, C.A., Pan, J., Yu, K., Zhang, L., Ornitz, D.M., 2010. Analysis of a gain-of-function FGFR2 Crouzon mutation provides evidence of loss of function activity in the etiology of cleft palate. Proc Natl Acad Sci U S A 107, 2515-2520.
Soga , K., Abo , H., Qin , S.-Y., Kyoutou , T., Hiemori , Tateno , Matsumoto , N., Hirabayashi, J., Yamamoto, K., 2015. Mammalian cell surface display as a novel method for developing engineered lectins with novel characteristics. Biomolecules 5, 1540-1562.
Sonnichsen, B., Lowe, M., Levine, T., Jamsa, E., Dirac-Svejstrup B, e.a., 1998. A role for giantin in docking COPI vesicles to Golgi membranes. J Cell Biol 140, 1013-1021.
Takahara, S., Takigawa, T., Shiota, K., 2004. Programmed cell death is not a necessary prerequisite for fusion of the fetal mouse palate. Int J Dev Biol 48, 39-46.
Tollefsen, S.E., Kornfeld, R., 1983. The B4 lectin from Vicia villosa seeds interacts with N-acetylgalactosamine residues alpha-linked to serine or threonine residues in cell surface glycoproteins. J. Biol. Chem 258, 5172-5176.
Valerius, M.T., Patterson, L.T., Witte, D.P., Potter, S.S., 2002. Microarray analysis of novel cell lines representing two stages of metanephric mesenchyme differentiation. Mech Dev 110, 151-164.
Vigetti, D., Genasetti, A., Karousou, E., Viola, M., Clerici, M., Bartolini, B., Moretto, P., De Luca, G., Hascall, V.C., Passi, A., 2009. Modulation of hyaluronan synthase activity in cellular membrane fractions. J. Bio Chem 284.
Wang, H., Yang, H., Shivalila, C.S., Dawlaty, M.M., Cheng, A.W., Zhang, F., Jaenisch, R., 2013. One-step generation of mice carrying mutations in multiple genes by CRISPR/Cas-mediated genome engineering. Cell 153, 910-918.
Wong, M., Munro, S., 2014. Membrane trafficking. The specificity of vesicle traffic to the Golgi is encoded in the golgin coiled-coil proteins. Science 346, 1256898.
Xiang, Y., Zhang, X., Nix, D.B., Katoh, T., Aoki, K., Tiemeyer, M., Wang, Y., 2013. Regulation of protein glycosylation and sorting by the Golgi matrix proteins GRASP55/65. Nat Commun 4, 1659.

Xu, J., Liu, H., Lan, Y., Aronow, B.J., Kalinichenko, V.V., Jiang, J., 2015. A Shh-Foxf-Fgf18-Shh molecular circuit regulating palate development. PLoS Genet.
Xu, J., Liu, H., Park, J.S., Lan, Y., Jiang, R., 2014. Osr1 acts downstream of and interacts synergistically with Six2 to maintain nephron progenitor cells during kidney organogenesis. Development 141, 1442-1452.
Yu, H., Smallwood, P.M., Wang, Y., Vidaltamayo, R., Reed, R., Nathans, J., 2010. Frizzled 1 and frizzled 2 genes function in palate, ventricular septum and neural tube closure: general implications for tissue fusion processes. Development 137, 3707-3717.
Zhong, W., 2011. Golgi during development. Cold Spring Harb Perspect Biol 3, a005363.
Zhou, J., Gao, Y., Lan, Y., Jia, S., Jiang, R., 2013. Pax9 regulates a molecular network involving Bmp4, Fgf10, Shh signaling and the Osr2 transcription factor to control palate morphogenesis. Development 140, 4709-4718.

Figures

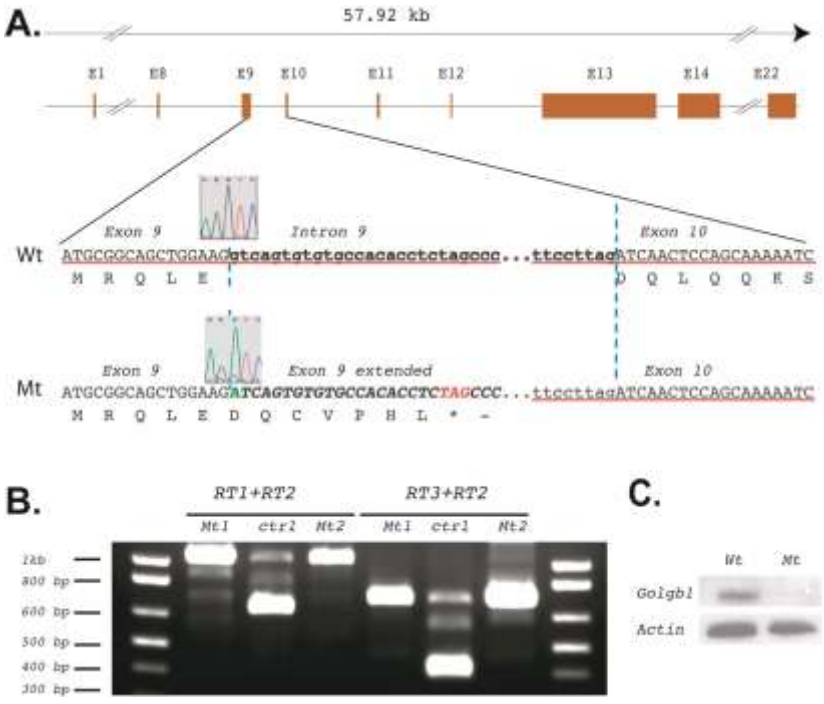

Fig. 1. The *ENU1483* mice carry a splice donor site mutation that disrupts *Golgb1* mRNAs and fail to produce Golgb1 protein. (A) Schematic depiction of the intron-9 splice donor mutation in *Golgb1*. (B) RT-PCR analysis shows that *Golgb1* mutant (Mt1 and Mt2) embryos express aberrantly spliced *Golgb1* mRNAs compared to control (ctrl) embryos. (C) Western blot assay shows that homozygous mutant (Mt) embryos failed to produce Golgb1 protein. β-Actin was detected for quantitative comparison between the samples.

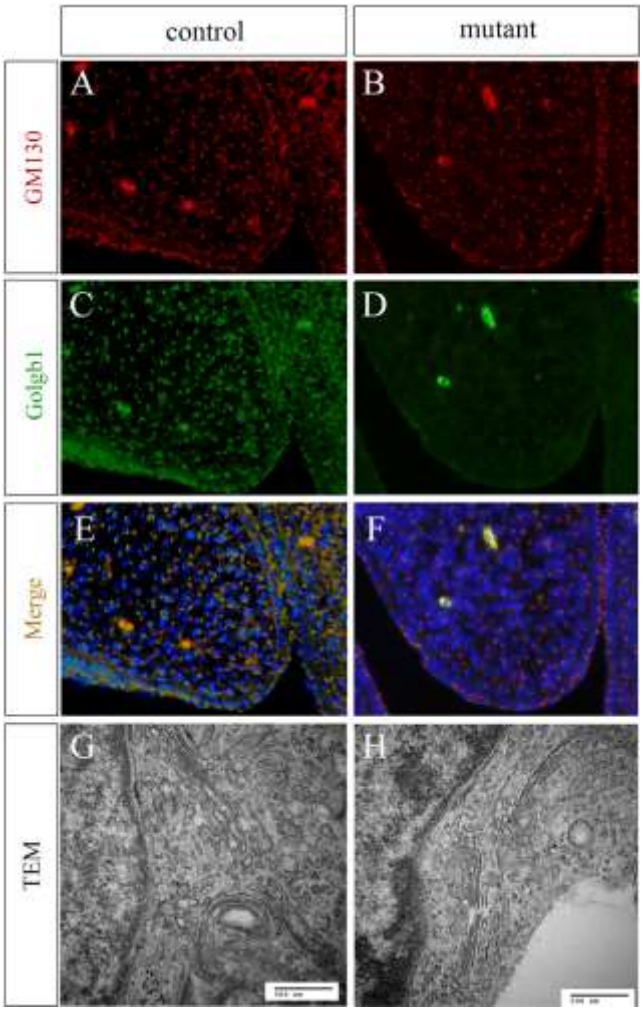

Fig. 2. Immunofluorescent detection of Golgb1 protein and electron microscopy analysis of Golgi structure. (A-F) Double immunofluorescent detection of GM130 (red, A and B) and Golgb1 (green, C and D) on frontal sections through the palatal shelves of E13.5 *Golgb1*$^{ivs9+1G>A/+}$ heterozygous (A, C, E) and homozygous mutant (B, D, F) embryos (n=9). (G, H) Transmission electron microscopy analysis of Golgi structure in palatal mesenchyme cells from E14.0 heterozygous (G) and homozygous mutant (H) embryos (n=4). Scale bar in G and H, 500 nm.

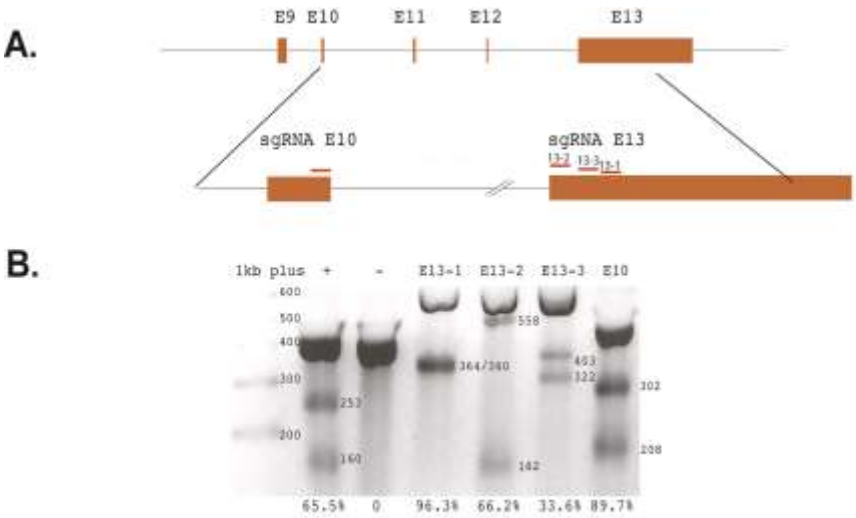

C.

E10 5' TTTACCAGATGTTAATAATGAGGGCGAGCAG 3'

#9 (F)	5' TTTACCAGA(ataataa)TAATAATGAGGGCGAGCAG	3' (3bp deletion & 7bp insertion)
#12(F)	5' TTTACCAGA--TTAATAATGAGGGCGAGCAG	3' (2bp deletion)
#20(M)	5' TTTACCAGAT----(ta)AATGAGGGCGAGCAG	3' (6bp deletion & 2bp insertion)
#35(F)	5' TTTACCAGAT(aa)TTAATAATGAGGGCGAGCAG	3' (1bp deletion & 2bp insertion)

All cause immediate premature STOP (TAA codon) of translation.

E13-1 5'GCAGGGCAAGAGGCCCGAGGGGGACTATGAGGTCCTCGACCGTAGAGAAGTGCAGCTGA 3'

#4 (M)	5'GCAGGGCAAGAGGCCCGAGGGGGACTATGAGGTCCT----CGTAGAGAAGTGCAGCTGA 3'	(4 bp deletion)
#8 (M)	5'GCAGGGCAAGAGGC----------CCGTAGAGAAGTGCAGCTGA 3'	(25 bp deletion)
#25(F)	5'GCAGGGCAAGAGGC----------CCGTAGAGAAGTGCAGCTGA 3'	(25 bp deletion)
#30(M)	5'GCAGGGCAAGAGGCCCGAGGGGGACTATGAGGTCCTCGA--GTAGAGAAGTGCAGCTGA 3'	(2 bp deletion)
#33(F)	5'GCAG----------AGAAGTGCAGCTGA 3'	(41 bp deletion)

E10-13 deletion

#17(M) carried a 11302 bp deletion which was predicted to result in in-frame 137 amino acid residues deletion in the protein product.

Fig. 3. Generation of new *Golgb1* mutant mice using CRISPR/Cas9 mediated genome editing. (A) Schematic diagram of the exon-9 to exon-13 region of the *Golgb1* gene. Red boxes represent exons. Target sites in exon-10 and exon-13, respectively, for the different sgRNAs are indicated. (B) SURVEYOR assay of PCR products from targeted genomic regions in transfected MK4 cells, with the ratio of altered versus wildtype DNA indicated below each lane. +, *Tet2* sgRNA was used as positive control. -, vector only as negative control. (C) Multiple mouse lines carrying various indel mutations were generated and indicated with the founder mouse number and gender.

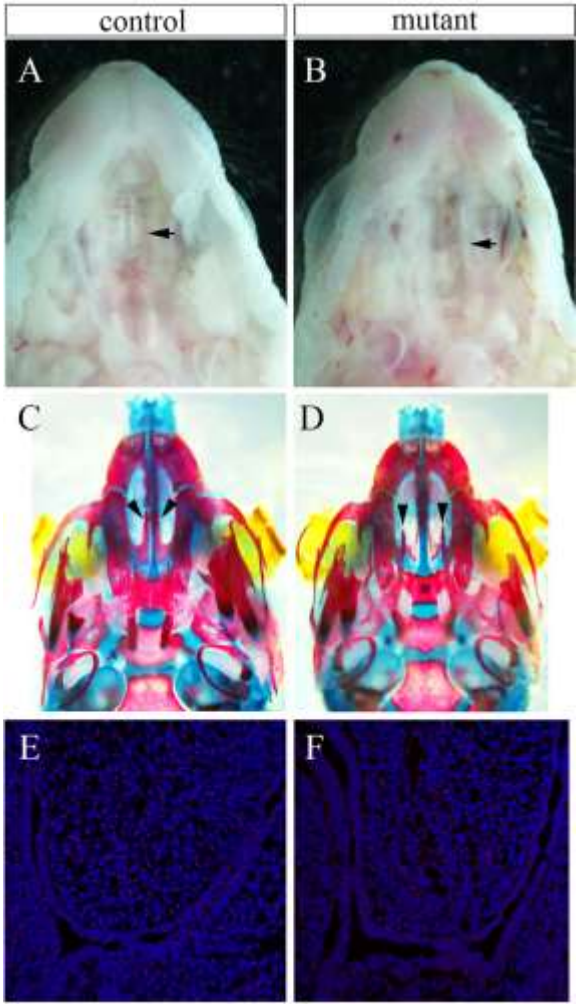

Fig. 4. Loss of *Golgb1* function causes cleft palate in mice. (A, B) Newborn mice trans-heterozygous for *Golgb1*$^{ivs9+1G>A}$ and *Golgb1*$^{E13-41bp}$ alleles exhibit cleft palate (B) (n=6) in comparison with *Golgb1*$^{ivs9+1G>A/+}$ littermates (A). Arrowhead points to the midline of the palate. (C, D) Skeletal preparations of E18.5 pups show that a *Golgb1*$^{ivs9+1G>A/E13-4bp}$ trans-heterozygous pup (D) had laterally displaced palatine processes of the maxillary and palatine bones, compared with a control littermate (C). Arrowheads point to the palatine processes of the maxillary bone and * in D marks the presphenoid bone. (E, F) Immunofluorescent detection of Golgb1 protein (red color) on frontal sections of E13.5 wildtype (E) and *Golgb1*$^{E13-25bp}$ homozygous mutant (F) embryos (n=9). All sections were counterstained with DAPI to visualize the cell nuclei (blue color).

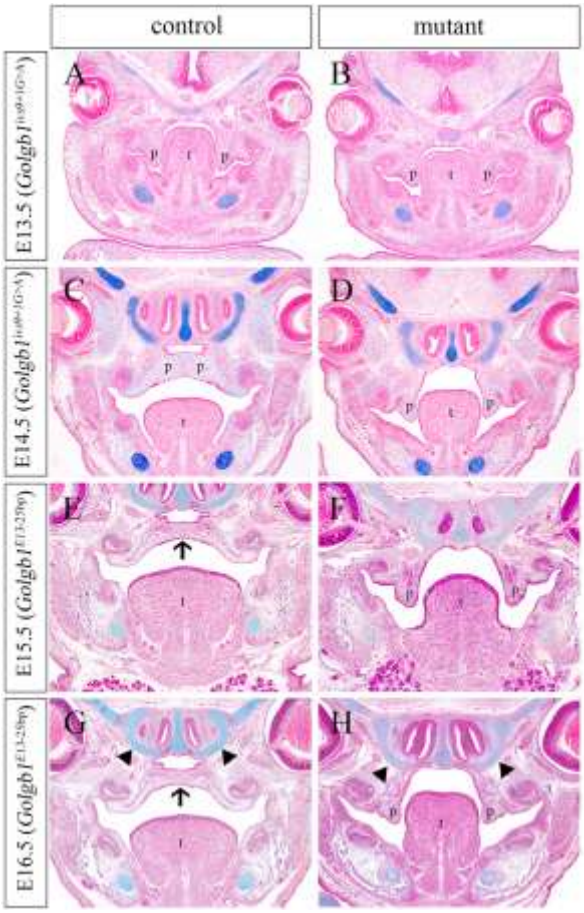

Fig. 5. *Golgb1* mutant embryos exhibit failure of palatal shelf elevation. (A-D) Frontal sections through the middle region of E13.5 (A, B) (n=8) and E14.5 (C, D) (n=6) *Golgb1*$^{ivs9+1G>A}$ heterozygous (A, C) and homozygous (B, D) embryos. (E-H) Frontal sections through the middle region of E15.5 (A, B) (n=5) and E16.5 (C, D) (n=5) *Golgb1*$^{E13-25bp}$ heterozygous (E, G) and homozygous (F, H) embryos. Arrows in E and G point to the fused midline of the secondary palate. Arrowheads in G and H point to nasal cartilages. p, palatal shelf; t, tongue.

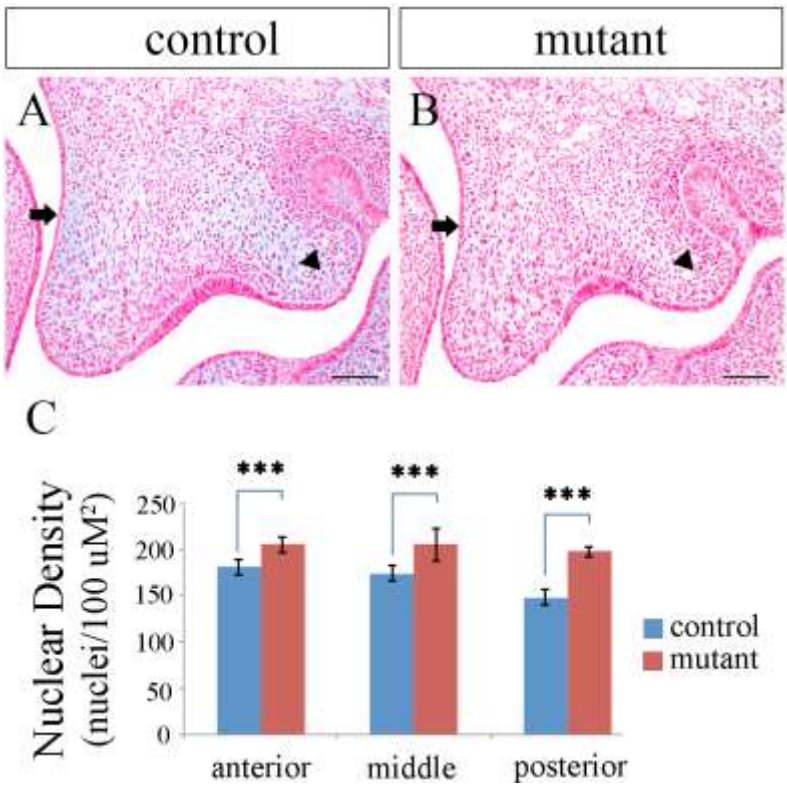

Fig. 6. The *Golgb1* mutant embryos exhibit decreased GAG accumulation and increased cell density in the palatal mesenchyme (A, B) HE and alcian blue stained frontal sections from the middle region of the palatal shelves of E13.5 *Golgb1*$^{ivs9+1G>A}$ heterozygous (A) and homozygous mutant (B) embryos (n=9). Arrow points to nasal side of the palatal mesenchyme while arrowhead marks the hinge area of the palatal shelves. (C) Quantification of nuclear density from DAPI-stained serial frontal sections of E13.5 *Golgb1*$^{E13\text{-}25bp}$ homozygous mutant and control littermates. Data were analyzed using 5 pairs of mutant and control embryos. Error bars represent standard deviation. ***, $p < 0.001$.

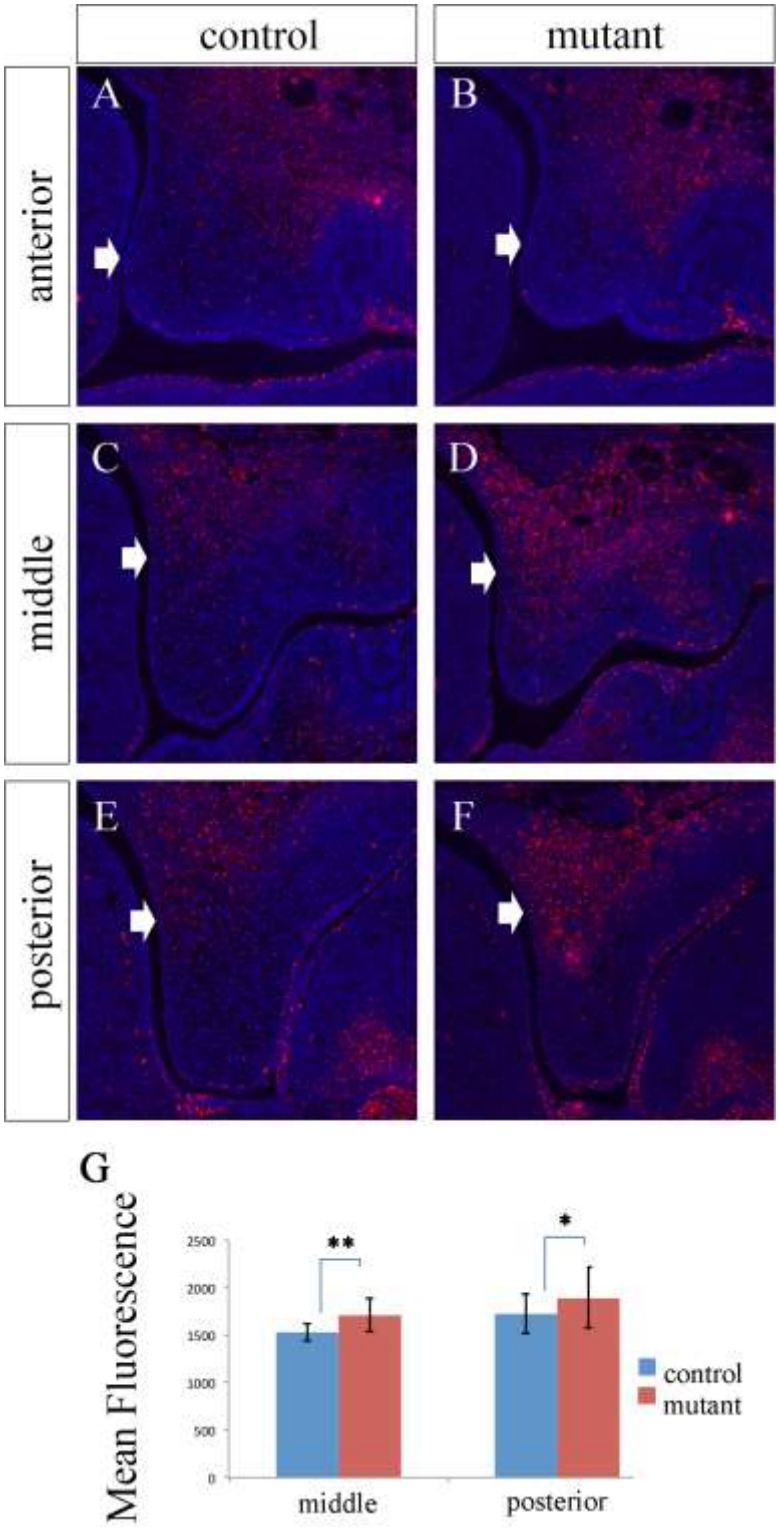

Fig. 7. The *Golgb1* mutant embryos exhibit significantly reduced hyaluronan accumulation in the palatal mesenchyme. (A-F) Serial frontal sections through the anterior (A, B), middle (C, D), and posterior (E, F) regions of the palatal shelves of E13.5 *Golgb1*$^{E13\text{-}25bp}$ heterozygous (A, C, E) and homozygous (B, D, F) littermates were stained with biotin-labeled HABP and detected using Texas-red fluorescence (n=6). Arrow points to the nasal side of the palatal shelf. (G) Quantification of mean fluorescence intensity in the HABP stained palatal shelf regions in the *Golgb1*$^{E13\text{-}25bp}$ homozygous mutant and heterozygous control samples. *, $p < 0.05$; ***, $p < 0.001$.

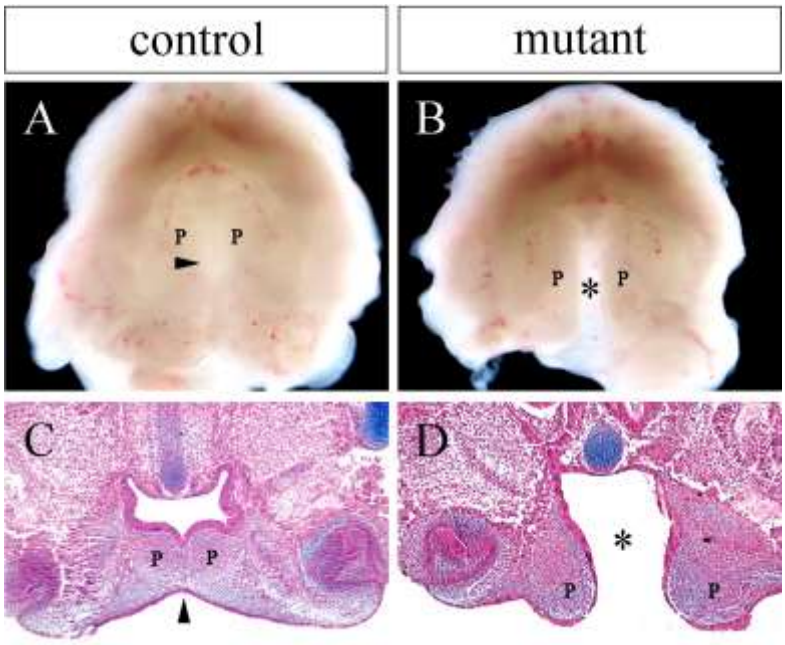

Fig. 8. Analysis of palatal shelf elevation using maxillary explant culture. (A, B) whole mount oral view of cultured wildtype (A) and *Golgb1*$^{E13\text{-}25bp}$ homozygous mutant (B) maxillary explants (n=8). (C, D) Frontal sections of cultured wildtype (C) and *Golgb1*$^{E13\text{-}25bp}$ homozygous mutant (D) maxillary explants. Arrowhead in C points to fusion between the palatal shelves at the midline. * in D marks the gap between the palatal shelves. p, palatal shelf.

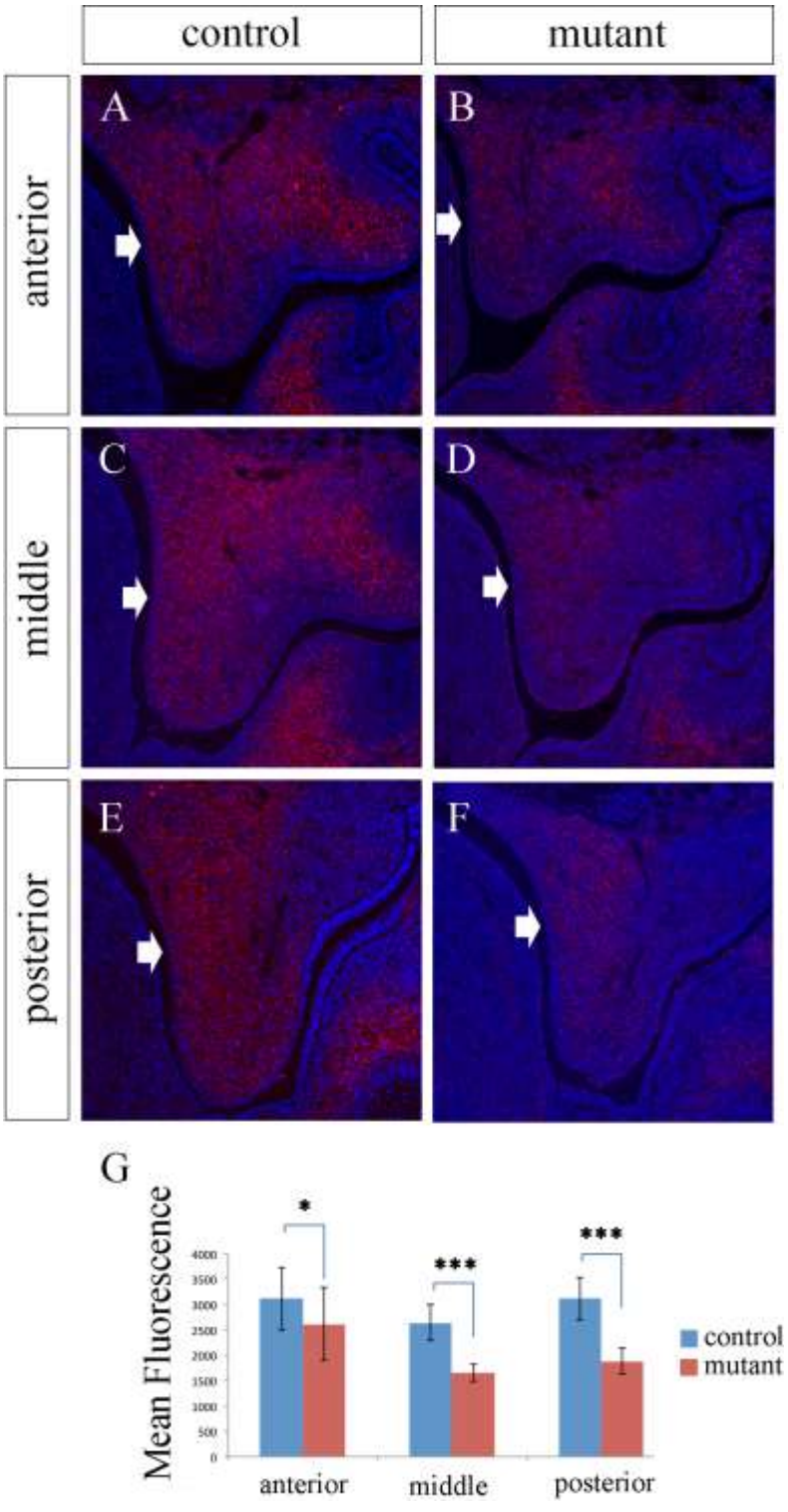

Fig. 9. Detection of glycosylation defect in the *Golgb1* mutant palatal tissues using

Lectin GSII staining. (A-F) Frontal sections through the anterior (A, B), middle (C, D), and posterior (E, F) regions of palatal shelves of E13.5 *Golgb1*$^{E13\text{-}25bp}$ heterozygous (A, C, E, n=4) and homozygous (B, D, F, n=4) littermates were stained with Alexa-594 conjugated GSII Lectin (red fluorescence). Arrow points to the nasal side of the palatal shelf. (G) Quantification of the mean fluorescence intensity across the middle and posterior palatal shelf sections from 4 pairs of control and mutant embryos. *, $p < 0.05$; **, $p < 0.01$.

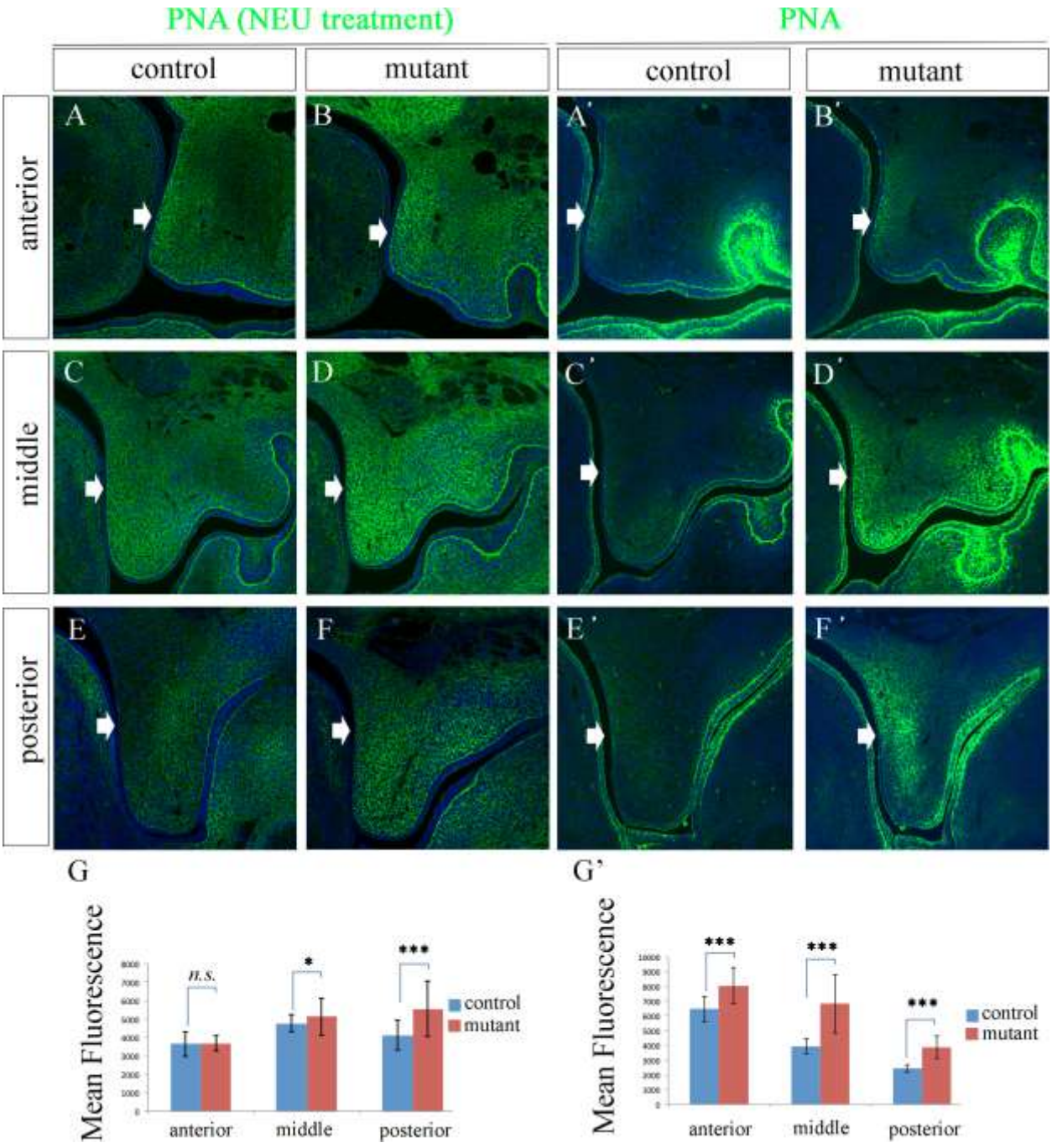

Fig. 10. Detection of PNA binding to frontal sections of developing palatal shelves. (A–F and A'-F') Frontal sections through the anterior (A, B, A', B'), middle (C, D, C', D') and posterior (E, F, E', F') regions of the palatal shelves of control (A, C, E, A', C', E', n=6) and

homozygous mutant (B, D, F, B', D', F', n=6) embryos were stained with fluorescein-conjugated PNA with (A-F) or without (A'-F') pretreatment with neuraminidase. White arrow point to nasal side of the palatal shelf in each panel. (G, G') Quantification of mean fluorescence intensity across PNA-stained palatal shelf regions from three pairs of control and mutant littermates. n.s., difference not statistically significant ($p > 0.05$); *, $p < 0.05$; ***, $p < 0.001$.

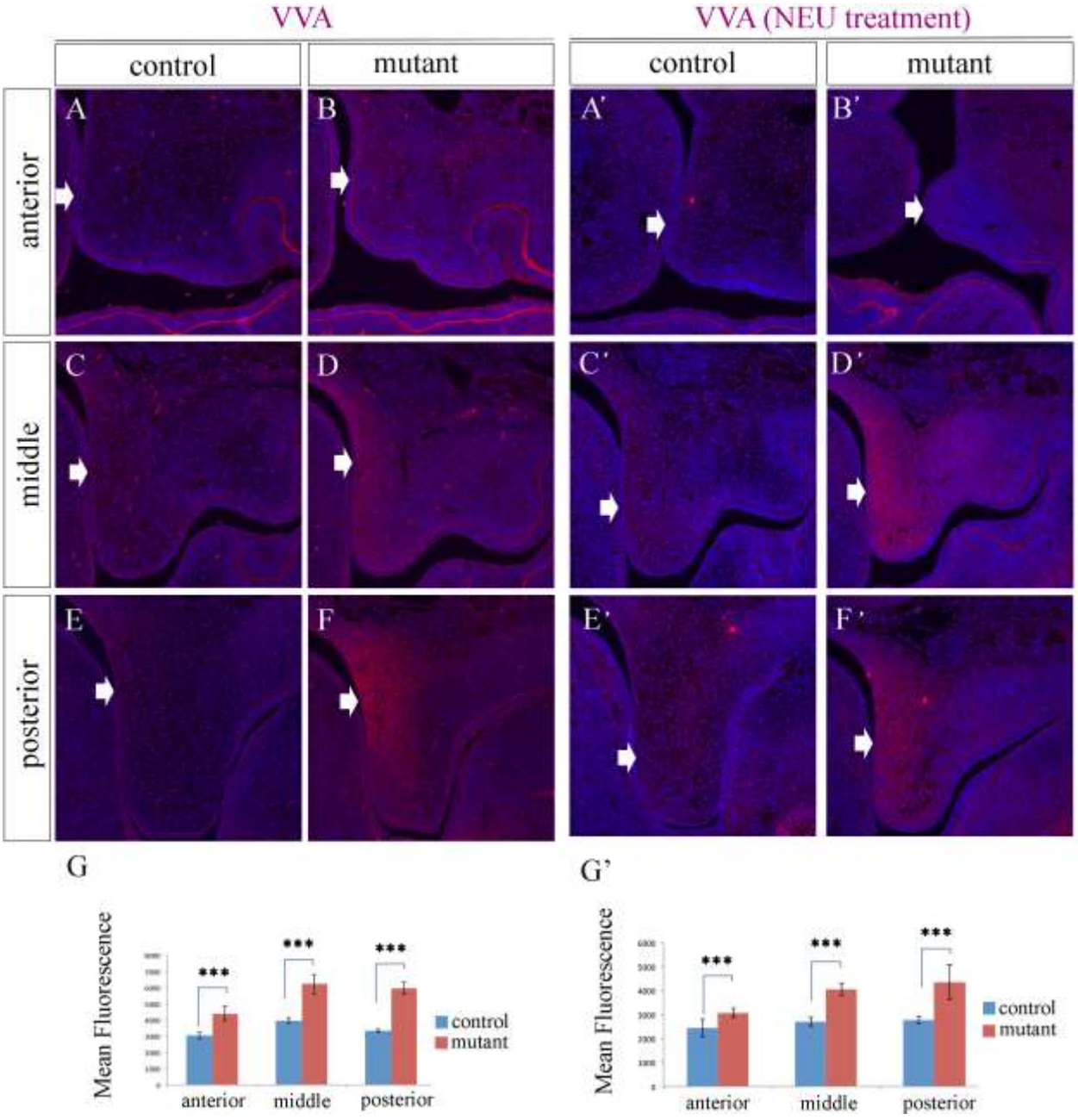

Fig. 11. Detection of glycosylation defects in palatal mesenchyme using VVA lectin staining. (A-F and A'-F') Frontal sections through the anterior (A, B, A', B'), middle (C, D, C', D'), and posterior (E, F, E', F') regions of the palatal shelves of E13.5 *Golgb1*$^{E13\text{-}25bp}$ heterozygous (A, C, E, A', C', E') and homozygous (B, D, F, B', D', F') littermates were stained

with VVA lectin (red fluorescence) without (A-F) or with (A'-F') pretreatment with neuraminidase. Arrow points to nasal side of the palatal shelf. (G, G') Bar graphs showing comparison of mean fluorescence intensity in the VVA stained palatal shelf regions from 3 pairs of *Golgb1*$^{E13\text{-}25bp}$ homozygous mutant and heterozygous control samples. ***, $p < 0.001$.

Supplementary Table 1. Genetic linkage of cleft palate in *ENU1483* mice to mouse Chromosome 16 [a]

SNP Name	Chr	Location	FVB	A/J[b]	CP1	CP2	CP3	CP4	CP5	CP6	CP7	CP8	CP9
JAX00067826	16	29499546	CC	TT	TT	TC	TC	TT	TT	TT	TT	TC	TT
UNC160278519	16	38863625	CC	TT	TT	TT	TT	TT	TT	TT	TT	TT	TT
JAX00418958	16	42099788	CC	TT	TT	TT	TT	TT	TT	TT	TT	TT	TT
JAX00419820	16	46687870	CC	TT	TT	TT	TT	TT	TT	TT	TT	TT	TT
UNC160215464	16	47168456	CC	TT	TT	TT	TT	TT	TT	TT	TT	TT	TT
UNC160074498	16	50520270	CC	TT	TT	TT	TT	TT	TT	TT	TT	TT	TT
JAX00421033	16	52729511	CC	TT	TC	TT	TC	TT	TC	TT	TC	TT	TC
UNC160349027	16	54655050	CC	TT	TC	TT	TC	TT	TC	TT	TC	TT	TC

[a] Genetic linkage mapping was performed using the mouse universal genotyping array single nucleotide polymorphism (SNP) microarray (GeneSeek, Inc.). This table only lists C/T variants between the parental strains in the chromosome 16 region that cosegregated with cleft palate in all nine G3 pups (CP1 – CP9).

Supplementary Table 2. ENU-induced mutations associated with cleft palate in *ENU1483* mutant mice

Gene	Chromosome	Position	Reference	Alternate	Codon Changes	AA Changes	Impact	ENU1483 Genotype
Itgb5	chr16	33948816	C	T	tCc/tTc	S793F	Moderate	homozygous
Adcy5	chr16	35156719	G	A	Ggc/Agc	G179S	Moderate	homozygous
Golgb1	Chr16	36898994	G	A	III	Intron (splice donor)	High	homozygous

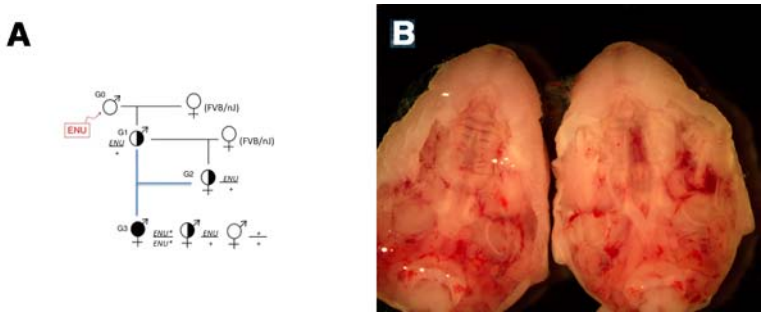

Supplementary Fig. 1. Screening for recessive birth defect mutations in mice using ENU mutagenesis. (A) Outline of the three-generation recessive mutation screening strategy. G0 A/J male mice are treated with ENU and crossed to FVB/NJ female mice to establish G1 males, which are crossed to FVB/NJ females to establish distinct G1 families. In each G1 family, timed mating of the G2 females with the G1 male were set up and pregnant G2 females euthanized in late gestation to screen G3 embryos for defects in external morphology and internal organs. (B) Upper jaws of two E18.5 G3 embryos are shown. one had normal palate while the other had cleft palate.

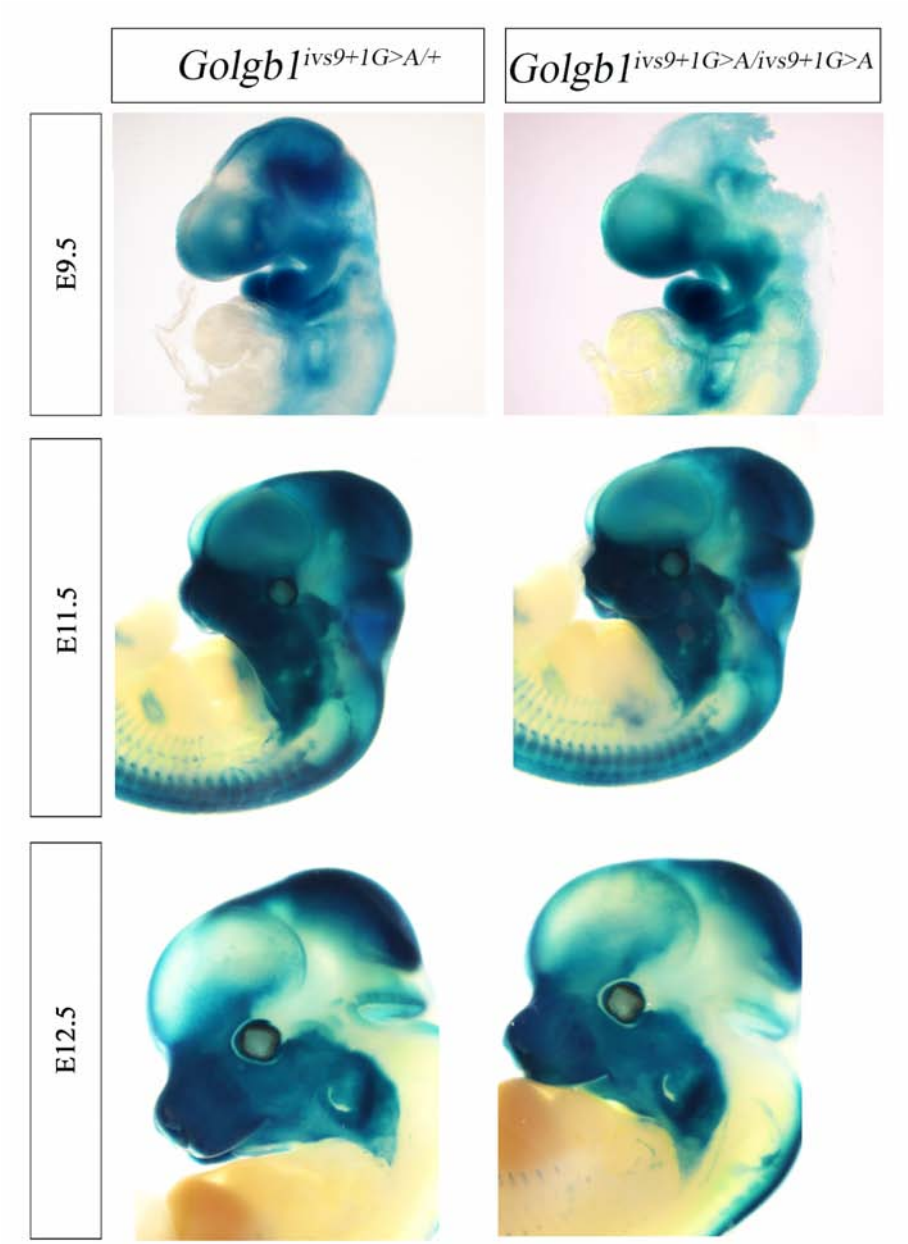

Supplementary Fig. 2. The *Golgb1*$^{ivs9+1G>A}$ homozygous mutant embryos exhibit normal neural crest migration and contribution to the facial primordia. Representative X-gal stained *R26R;Wnt1Cre; Golgb1*$^{ivs9+1G>A/+}$ heterozygous control (left column) and *R26R;Wnt1Cre; Golgb1*$^{ivs9+1G>A/ivs9+1G>A}$ mutant (right column) embryos at E9.5 (top row), E11.5 (middle row), and E12.5 (bottom row) are shown. Blue color in the facial regions indicate neural crest-derived mesenchyme. No consistent differences were detected between the different genotypes in any litter.

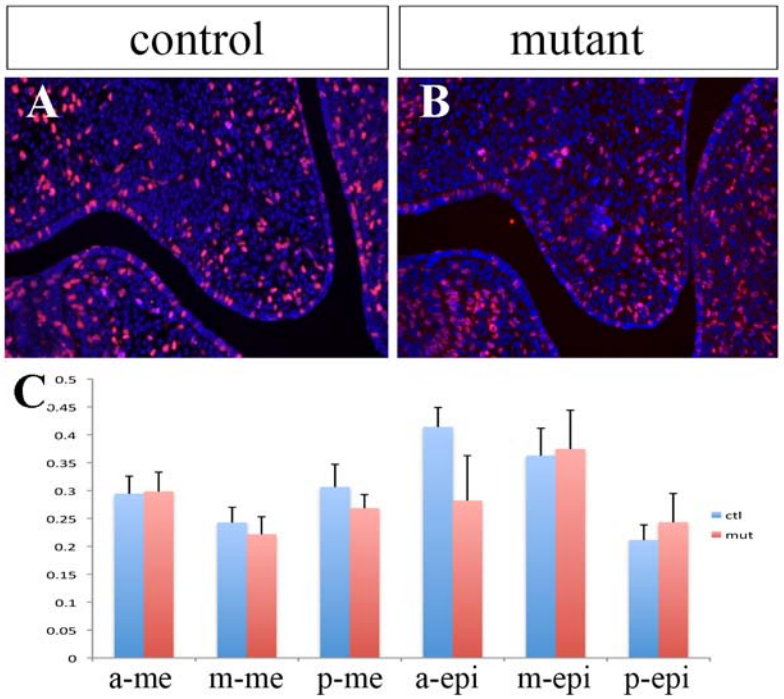

Supplementary Fig. 3. Comparison of palatal cell proliferation index in the E13.5 *Golgb1*$^{ivs9+1G>A}$ homozygous mutant and control littermates. (A, B) Representative photographs showing BrdU-labeled cell nuclei (red color) on frontal sections of the palatal shelves of heterozygous control (A) and homozygous mutant (B) embryos. All cell nuclei are counterstained with DAPI and shown in blue color. (C) The percentage of BrdU labeled cells (1 equals 100%) were calculated separately for the palatal epithelium and mesenchyme in each of the anterior, middle, and posterior regions of the palatal shelves. No significant difference was detected in either the palatal epithelium or mesenchyme in any region of the palatal shelves between the control and homozygous mutant embryos. a, anterior; m, middle; p, posterior; epi, epithelium; me, mesenchyme.

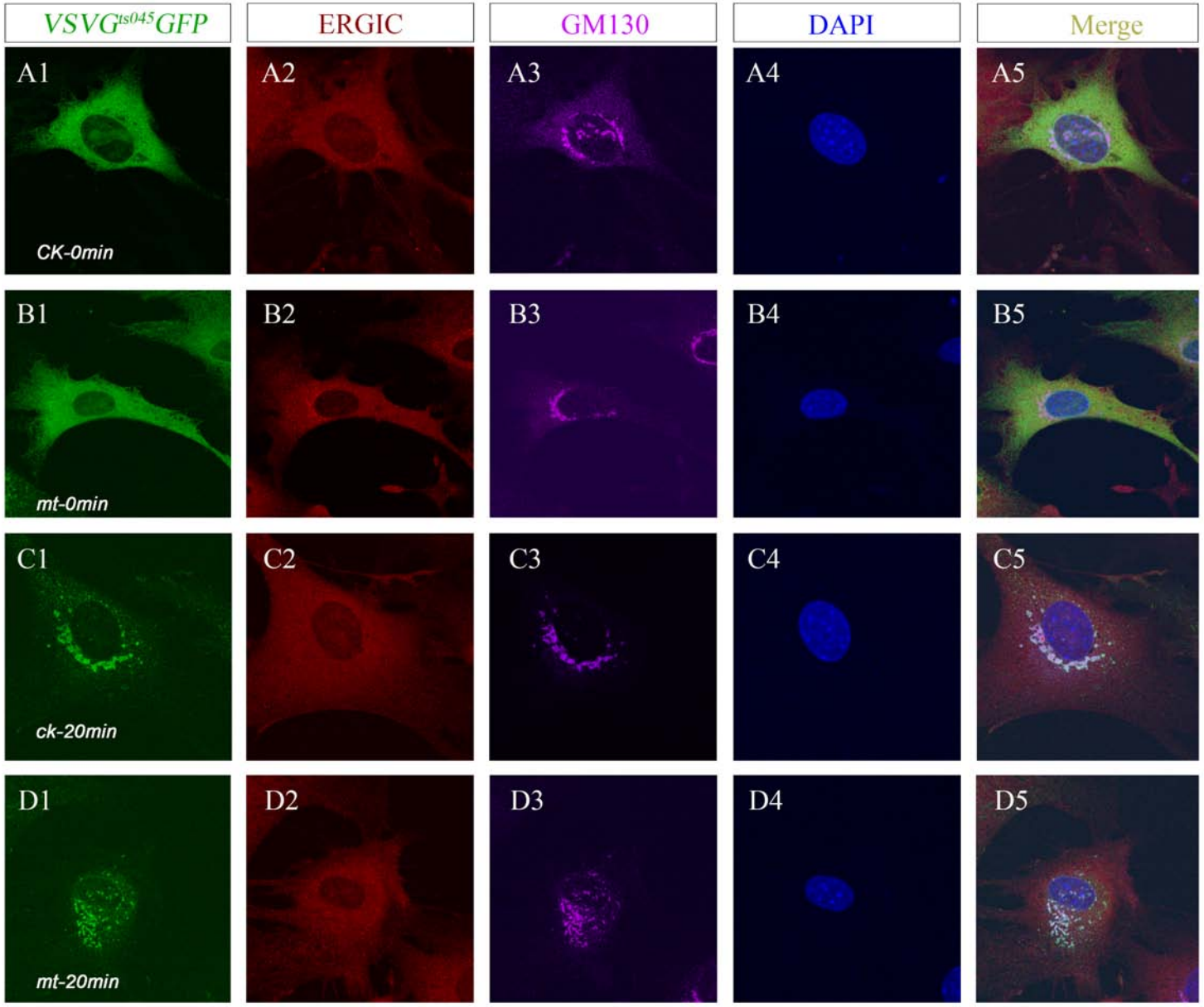
VSVG^ts045GFP
ERGIC
GM130
DAPI
Merge
A1
A2
A3
A4
A5
CK-0min
B1
B2
B3
B4
B5
mt-0min
C1
C2
C3
C4
C5
ck-20min
D1
D2
D3
D4
D5
mt-20min

Supplementary Fig. 4. Analysis of ER-to-Golgi transport of the VSVG^{ts045}-GFP reporter protein in palatal mesenchyme cells isolated from E13.5 *Golgb1*$^{ivs9+1G>A}$ homozygous mutant and heterozygous control embryos. Each row shows one representative cell imaged for the GFP reporter (1st column from left, shown in green color), ERGIC immunofluorescence (2nd column, shown in red color), GM130 immunofluorescence (3rd column, shown in purple color), DAPI (4th column, shown in blue color), and merged picture (5th column). (A, B) Control (A) and mutant (B) cells cultured at the restrictive temperature (40 ^{o}C) and fixed for immunofluorscent staining. (C, D) Control (C) and mutant (D) cells were shifted from 40 ^{o}C to 32 ^{o}C for 20 minutes and fixed for immunofluorescent staining.